Differentiation signals induce *APOBEC3A* expression via GRHL3 in squamous epithelia and squamous cell carcinoma

Nicola J. Smith[1,2,†], Ian Reddin[1,3,†], Paige Policelli[1,4], Sunwoo Oh[5], Nur Zainal[1], Emma Howes[1], Benjamin Jenkins[1], Ian Tracy[1], Mark Edmond[1], Benjamin Sharpe[1], Damian Amendra[1], Ke Zheng[6], Nagayasu Egawa[6], John Doorbar[6], Anjali Rao[7], Sangeetha Mahadevan[7], Michael A. Carpenter[8,9], Reuben S. Harris[8,9], Simak Ali[10], Christopher Hanley[1], Rémi Buisson[5], Emma King[1], Gareth J. Thomas[1,11], Tim R. Fenton[1,11,*]

[1] School of Cancer Sciences, Faculty of Medicine, University of Southampton, UK

[2] School of Biosciences, University of Kent, UK

[3] Bio-R Bioinformatics Research Facility, Faculty of Medicine, University of Southampton, UK

[4] Cell, Gene and RNA Therapies, Discovery Sciences, BioPharmaceuticals R&D, AstraZeneca, Cambridge, UK.

[5] Department of Biological Chemistry, School of Medicine, University of California Irvine, Irvine, CA, USA

[6] Department of Pathology, University of Cambridge, UK

[7] Gilead Sciences, Research Department, 324 Lakeside Dr. Foster City, CA 94404, USA

[8] Department of Biochemistry and Structural Biology, University of Texas Health San Antonio, San Antonio, TX 78229, USA

[9] Howard Hughes Medical Institute, University of Texas Health San Antonio, San Antonio, TX 78229, USA

[10] Department of Surgery and Cancer, Imperial College London, Hammersmith Hospital Campus, London, UK.

[11] Institute for Life Sciences, University of Southampton, UK

[†] Equal contribution

* Correspondence to t.r.fenton@soton.ac.uk

Abstract

Two APOBEC DNA cytosine deaminase enzymes, APOBEC3A and APOBEC3B, generate somatic mutations in cancer, thereby driving tumour development and drug resistance. Here, we used single-cell RNA sequencing to study *APOBEC3A* and *APOBEC3B* expression in healthy and malignant mucosal epithelia, validating key observations with immunohistochemistry, spatial transcriptomics and functional experiments. Whereas *APOBEC3B* is expressed in keratinocytes entering mitosis, we show that *APOBEC3A* expression is confined largely to terminally differentiating cells and requires grainyhead-like transcription factor 3 (GRHL3). Thus, in normal tissue, neither deaminase appears to be expressed at high levels during DNA replication, the cell-cycle stage associated with APOBEC-mediated mutagenesis. In contrast, in squamous cell carcinoma we find that, there is expansion of *GRHL3*expression and activity to a subset of cells undergoing DNA replication and concomitant extension of *APOBEC3A* expression to proliferating cells. These findings suggest that APOBEC3A may play a functional role during keratinocyte differentiation, and offer a mechanism for acquisition of APOBEC3A mutagenic activity in tumours.

Keywords

APOBEC3A, cancer mutagenesis, GRHL3, keratinocyte, HNSCC

Introduction

The *APOBEC3A* and *APOBEC3B* (apolipoprotein B mRNA editing catalytic polypeptide-like 3A and 3B) genes encode two closely related DNA cytosine deaminases that belong to the seven-protein human APOBEC3 family. The APOBEC3 enzymes convert deoxycytidine to deoxyuridine in single-stranded DNA (ssDNA), a mutagenic activity that explains at least in part their ability to restrict replication of retroviruses and endogenous retroelements through targeting nascent cDNA during reverse transcription (Harris & Dudley, 2015; Conticello, 2008). In addition, APOBEC3A and APOBEC3B have evolved functions in the cell nucleus including transcriptional regulation (Periyasamy *et al*, 2015; Taura *et al*, 2022) and responses to nuclear-resident viruses (Chen *et al*, 2006; Vartanian *et al*, 2008; Warren *et al*, 2015; Lejeune *et al*, 2023; Lucifora *et al*, 2014; Cheng *et al*, 2018). Acquisition of these nuclear functions appears to have come at a cost however, as both APOBEC3A and APOBEC3B have been implicated in generating somatic mutations (mainly C>T transitions and C>G tranversions at TpC sites) in cancer cell genomes, driving cancer development and therapeutic resistance (Henderson & Fenton, 2015; Swanton *et al*, 2015; Petljak & Maciejowski, 2020; Mertz *et al*, 2022; Green & Weitzman, 2019; Isozaki *et al*, 2023; Lin *et al*, 2022; Caswell *et al*, 2023; Periyasamy *et al*, 2020; Law *et al*, 2020; Durfee *et al*, 2023; Naumann *et al*, 2023). Two mutation signatures attributed to APOBEC3A/B activity have been observed in multiple cancer types but although extensive biochemical and genetic data support the involvement of both APOBEC3A and APOBEC3B in somatic mutagenesis, their gene expression levels as determined by analysis of bulk tumour data or in cancer cell lines that display the signatures are only weakly, if at all, correlated with the presence of these mutation signatures (Alexandrov *et al*, 2013; Roberts *et al*, 2013; Burns *et al*, 2013b, 2013a; Taylor *et al*, 2013; Cortez *et al*, 2019; Buisson *et al*, 2019; Jalili *et al*, 2020; Petljak *et*

al, 2022a). Accurately determining the conditions under which *APOBEC3A* and *APOBEC3B* are expressed in normal and cancerous tissues represents a key challenge in building our understanding of how APOBEC-mediated mutagenesis occurs, and how they might be targeted for cancer treatment (Petljak *et al*, 2022b). This objective is complicated however, by their expression in immune cells, which are frequently present at high levels in tumour biopsies, and until recently by a lack of specific antibodies for *in situ* analysis. Here, we addressed these challenges by conducting single cell RNA sequencing (scRNA-seq) of matched normal and tumour samples from patients with head and neck squamous cell carcinoma (HNSCC), a tumour type in which high burdens of APOBEC signature mutations are frequently observed, with evidence pointing to roles for both APOBEC3A and APOBEC3B in generating these mutations (Alexandrov *et al*, 2013; Burns *et al*, 2013b; Roberts *et al*, 2013; Henderson *et al*, 2014; The Cancer Genome Atlas Network, 2015; Faden *et al*, 2017). We analysed *APOBEC3A* and *APOBEC3B* gene expression patterns in these data and in additional published scRNA-seq datasets from healthy and cancerous epithelial tissues, deploying recently developed antibodies in immunohistochemical analysis of tissue sections to corroborate our findings at the protein level. We used computational methods to predict transcription factors responsible for regulating APOBEC expression and validated our predictions in near-normal immortalized keratinocytes (NIKS) (Allen-Hoffmann *et al*, 2000), identifying Grainyhead-like transcription factor 3 (GRHL3) as a novel regulator of *APOBEC3A* expression in terminally differentiating keratinocytes. In contrast, and consistent with findings from different cell types (Hirabayashi *et al*, 2021; Roelofs *et al*, 2023), *APOBEC3B* expression is confined to proliferating cells, with highest levels evident in G2/M-phase of the cell cycle. In HNSCC, we find evidence of GRHL3 activity and *APOBEC3A* in a subpopulation of tumour cells undergoing DNA replication; the context in which mutagenic

APOBEC activity is postulated to occur due to deamination of lagging strand ssDNA exposed at the replication fork (Green *et al*, 2016; Haradhvala *et al*, 2016; Hoopes *et al*, 2016; Morganella *et al*, 2016; Seplyarskiy *et al*, 2016; Stewart *et al*, 2020). Our findings provide new insight into the transcriptional control of *APOBEC3A* gene expression in squamous epithelia and provide a potential mechanism for the acquisition of APOBEC3A-induced mutations in cancer.

Results

APOBEC3A is expressed in epithelial cells from healthy tonsil and oesophagus.

Although most cancers that display enrichment for APOBEC mutational signatures are carcinomas, i.e. tumours that arise from epithelial cells, little is known about the expression patterns and physiological regulation of *APOBEC3A* and *APOBEC3B* in healthy epithelium, or regarding the proportion of malignant cells that express *APOBEC3A*, *APOBEC3B* or both genes in tumour biopsies. To address these knowledge gaps, we assembled scRNA-seq data from the epithelial cells (see Methods) present in 10 oropharyngeal SCC samples and 7 matched normal (contralateral tonsil) samples from patients undergoing surgical resection at our institution (Table EV1), together with 11 published scRNA-seq datasets from healthy skin, breast and oesophagus and from cancers of the breast, bladder, head and neck (HNSCC), oesophagus (ESCC) and lung (all cancers that typically display moderate to strong enrichment for APOBEC mutation signatures, Table EV2). Very few *APOBEC3A* or *APOBEC3B* expressing epithelial cells were present in the normal skin, breast or lung datasets but 16.4% of epithelial cells from normal oesophagus and 38.1% from normal tonsil expressed *APOBEC3A*, 10.5% of which also expressed *APOBEC3B* (Fig 1). 3.5% of tonsil epithelial cells expressed only *APOBEC3B*, and the mean *APOBEC3A* expression per cell was significantly

higher than that of *APOBEC3B* in both tonsil and eosophagus (Fig 1, p<2.22E-16 (unpaired Wilcoxon's Rank Sum test)). In the tumour samples, the majority of epithelial (tumour) cells expressed neither *APOBEC3A* nor *APOBEC3B* at levels detectable by scRNA-seq, and the only datasets containing a significant number of cells expressing *APOBEC3A* and/or *APOBEC3B* were from HNSCC or ESCC (Fig 1). Only the datasets from healthy tonsil and oesophagus and from HNSCC and ESCC contained sufficient *APOBEC3A* and/or *APOBEC3B* expressing cells to permit further analysis, so we initially interrogated the data from tonsil epithelial cells, the dataset in which we observed the highest average *APOBEC3A* expression per cell and the greatest proportion of *APOBEC3A*- and/or *APOBEC3B*-positive cells (Fig 1).

APOBEC3A and _APOBEC3B_ are expressed in distinct cell sub-populations in healthy tonsil epithelium.

Since most *APOBEC3A*-expressing cells in the normal tonsil dataset did not co-express detectable levels of *APOBEC3B*, we were interested to determine whether the cells comprising this *APOBEC3A*-positive / *APOBEC3B*-negative population might share a common phenotype and if so, whether it might be distinct from the *APOBEC3A*-negative / *APOBEC3B*-positive, *APOBEC3A/B*-positive and *APOBEC3A/B*-negative populations. To address this question, after further quality control (see Methods for details), we identified the top 100 genes co-expressed with either *APOBEC3A* or *APOBEC3B* (Table EV3) in 2,649 epithelial cells from our healthy tonsil samples (Fig 2A, blue) and used pathway analysis to examine the gene ontology biological processes (GOBP) enriched among each geneset (Fig 2B). Considering only the top ten GOBP pathway hits for the two APOBECs, there was no overlap, and each was dominated by different biological processes. For *APOBEC3A* the top ten pathways included those involved in epidermal and keratinocyte development and

differentiation whereas, consistent with observations in bulk RNA-seq data from breast cancer (Cescon *et al*, 2015), all processes in the top ten for *APOBEC3B* were associated with mitosis (Fig 2B, Dataset EV1). This finding suggested that in healthy tonsil epithelium, *APOBEC3B* is expressed in cycling cells undergoing cell division while *APOBEC3A* is restricted to those keratinocytes undergoing terminal differentiation. To further investigate this possibility, the epithelial cells were clustered based on known markers for different epithelial cell states (Kang *et al*, 2015; Kabir *et al*, 2022; Rochman *et al*, 2022; Franzén *et al*, 2019). These genes included markers for basal cells (cytokeratin-14 (*KRT14*) and cytokeratin-15 (*KRT15*), proliferating epithelium (Ki-67 (*MKI67*), minichromosome maintenance complex component 7 (*MCM7*)), differentiating keratinocytes (involucrin (*IVL*), cytokeratin-10 (*KRT10*)), and terminally differentiating keratinocytes (*SPRR2A*, *S100P*) (Fig 2C, D). Similarly, scRNA-seq of healthy oesophageal epithelium (Madissoon *et al*, 2019) had previously been clustered into four distinct epithelial phenotypes: basal epithelium ('epi-basal'), a proliferating suprabasal epithelium ('epi-suprabasal'), differentiating stratified epithelium ('epi-stratified'), and terminally differentiated upper epithelium ('epi-upper') (Appendix Fig S1A). Marker gene expression patterns for these epithelial subtypes resembled those observed in the corresponding tonsillar epithelial subtypes (Appendix Fig S1B).

As inferred from the pathway analysis, *APOBEC3B* was expressed predominantly in proliferating cells, significantly more so than in differentiating cells ($p < 0.0001$, Wilcoxon's Rank Sum Test), exhibiting a similar expression profile to *MKI67* (Fig 2E). While also expressed in a subset of proliferating cells, *APOBEC3A* expression was significantly higher in differentiating cells ($p < 0.0001$, Wilcoxon's Rank Sum Test), and was also detectable in some terminally differentiated cells, following the expression pattern of *IVL* (Fig 2E).

Although *APOBEC3A* was expressed in a lower proportion of healthy oesophageal epithelial cells compared to those of the tonsillar epithelium, it was again co-expressed with *IVL* in differentiating cells and expressed weakly if at all, in the proliferative compartment ($p < 0.0001$, Wilcoxon's Rank Sum Test, Appendix Fig S1C).

Keratinocyte cell cycle exit and initiation of differentiation is marked by a switch from *APOBEC3B* to *APOBEC3A* expression.

Our finding that *APOBEC3A* is expressed in differentiating epithelial cells of the tonsil and oesophagus is consistent with a previous report that it is upregulated during Ca^{2+}-induced differentiation of W12 cells (a cell line established from a cervical neoplasia that harbours HPV16(Stanley *et al*, 1989)) and normal human epidermal keratinocytes (NHEK) (Wakae *et al*, 2018). In the same study, *APOBEC3B* upregulation was also observed in W12 cells following 10 days in high Ca^{2+} but not in NHEKs, suggesting an HPV-specific induction, as reported (Vieira *et al*, 2014; Henderson *et al*, 2014; Periyasamy *et al*, 2017). Ca^{2+} is an activator of protein kinase C (PKC) signalling, which also mediates potent induction of *APOBEC3A* by phorbol esters in keratinocytes (Rasmussen & Celis, 1993; Madsen *et al*, 1999; Siriwardena *et al*, 2018). We therefore sought to uncouple potential PKC-dependent effects from differentiation-dependent effects on *APOBEC3A* expression by using three other established methods for inducing keratinocyte differentiation: growth to high density; inhibition of epidermal growth factor receptor (EGFR); and growth factor withdrawal (Poumay & Pittelkow, 1995; Peus *et al*, 1997). In all three contexts we observed upregulation of *APOBEC3A*, along with *IVL* and *KRT10* and either no change (following 24 hours of the EGFR inhibitor afatinib) or a decrease (following growth to high density, serum and growth factor withdrawal) in *APOBEC3B* expression, closely mirroring decreases in

MKI67 and *MCM7* (Fig 3A, C, E). Analysis of DNA content by flow cytometry confirmed cell cycle arrest in all three conditions (Fig 3B, D, F). In contrast to *APOBEC3A* induction by phorbol 12-myristate 13-acetate (PMA), the upregulation observed following growth factor withdrawal was independent of PKC signalling (Appendix Fig S2A, B) and was also observed in primary keratinocytes (Figure 3G). Editing of cytosine 558 to uracil in the Dolichyl-diphosphooligosaccharide--protein glycosyltransferase 48 kDa subunit (DDOST) transcript (a highly specific measure of APOBEC3A deaminase activity (Jalili *et al*, 2020)) paralleled the increase in APOBEC3A mRNA observed upon growth factor withdrawal (Figure 3H). Upon treating NIKS with inhibitors of the two major mitogenic signalling pathways downstream of EGFR (RAS/MEK/ERK and PI3K/AKT/mTOR) we observed induction of *APOBEC3A* only by the MEK inhibitor trametinib, which was also the only compound to induce *IVL* / *KRT10* expression (Appendix Fig S2C, top) and to induce cell cycle arrest (Appendix Fig S2D). Interestingly the ERK1/2 inhibitor ravoxertinib did not block proliferation, nor did it induce *APOBEC3A* or differentiation markers (Appendix Fig S2C, D). PI3K (pictilosib), AKT (MK2206) and mTORC1 (everolimus) inhibitors had no effect on proliferation or *APOBEC3A* expression but they did reduce *APOBEC3B* expression, which unlike *MKI67* and *MCM7*, was unaffected by MEK inhibition (Appendix Fig S2C). PI3K inhibition has previously been shown to reduce *APOBEC3B* expression in the U2OS human osteosarcoma cell line, via effects on NFκB and AP-1 activity (Lin *et al*, 2020).

Taken together, our results from human tissue samples and the experiments in NIKS suggest that cell cycle exit and initiation of terminal differentiation in keratinocytes is accompanied by a switch in *APOBEC3* gene usage, from *APOBEC3B*, which is expressed in cycling cells entering cell division, to *APOBEC3A*.

APOBEC3A expression during keratinocyte differentiation requires Grainyhead-like transcription factor 3.

Transcription factor activity analysis of scRNA-seq data from normal tonsil epithelial cells using single-cell regulatory network inference and clustering (SCENIC) (Aibar *et al*, 2017) identified the Grainyhead-like transcription factor 3 (GRHL3), a key regulator of epidermal differentiation (Ting *et al*, 2005; Yu *et al*, 2006; Hopkin *et al*, 2012; Klein *et al*, 2017) as a potential regulator of *APOBEC3A* expression in the datasets from normal tonsil, HNSCC and ESCC, with strong positive associations between GRHL3 activity scores and *APOBEC3A* expression evident across all scRNA-seq datasets we analysed (Dataset EV2). Furthermore, GRHL3 was the only transcription factor among those whose activity was correlated with *APOBEC3A* expression, and significantly increased in the differentiating compartment of the normal tonsil epithelium, in which most *APOBEC3A*-expressing cells were clustered (Fig 4A, B, Fig 2E, Table EV4). It is also known to be activated downstream of the Receptor-Interacting Protein Kinase 4 (RIPK4) in PMA-treated keratinocytes (Scholz *et al*, 2016). Stratifying cells by their binary (on / off) GRHL3 activity as determined from SCENIC analysis (Appendix Fig S3) revealed increased *APOBEC3A* expression in 'GRHL3-on' cells (Fig 4C (upper panel); Wilcoxon's Rank Sum test $p<0.0001$). 936 of 1,416 (66%) 'GRHL3-on' cells expressed *APOBEC3A*, a significantly higher number of cells compared to those that were 'GRHL3-off', where only 73 of 1,233 (6%) cells expressed *APOBEC3A* (Fishers Exact Test, $p < 0.0001$; Fig 4C (lower panel)). Published GRHL3 target genes include *IVL* and E74 Like ETS Transcription Factor 3 (*ELF3*) (Scholz *et al*, 2016; Hopkin *et al*, 2012), both of which display very similar patterns of gene expression to *APOBEC3A* in response to differentiation stimuli in NIKS (Fig 3; Appendix Fig S2 and Appendix Fig S4). Suppressing *GRHL3* expression using

two different siRNAs blocked induction of *APOBEC3A* mRNA (Fig 4D) and DDOST mRNA editing (Fig 4E) by afatinib in NIKS, demonstrating a functional role for GRHL3 in activating *APOBEC3A* expression during differentiation. Induction of GRHL3 target genes *IVL* and *ELF3* was also suppressed, whereas expression of *MKI67* and *MCM7* was unaffected by *GHRL3* knockdown (Appendix Fig S5), consistent with GHRL3-dependent induction of *APOBEC3A* occurring during afatinib-induced differentiation, downstream of cell cycle exit. *GRHL3* knockdown also decreased *APOBEC3A* mRNA levels in PMA-treated NIKS (Appendix Fig S6A), and following growth factor withdrawal (Appendix Fig S6B, C). Analysis of chromatin immunoprecipitation (ChIP-seq) data from human keratinocytes (NHEK) (Hopkin *et al*, 2012; Klein *et al*, 2017) revealed GRHL3 binding at a predicted enhancer 33kb upstream of the *APOBEC3A* TSS following Ca^{2+}-induced differentiation but not in control (proliferating) cells, consistent with a direct role for GRHL3 in regulating *APOBEC3A* transcription (Fig 4F, Appendix Fig 7A, main panel). The 176 bp region at which the GRHL3 binding peak is located contains four 8-mer sequences that are close matches for the previously defined consensus GRHL3 binding motif (AACC[G/T]GTT) (Yu *et al*, 2006) (Appendix Fig 7A inset). GRHL3 has been shown to recruit the trithorax group (trxG) protein WDR5 to its target sites to enable H3K4 methylation (Hopkin *et al*, 2012), and a WDR5 binding peak coincided with the GRHL3 peak at -33kb in differentiating NHEKs (Fig 4F). A predicted promoter at -4kb relative to the TSS harbours NFκB and STAT2 binding sites previously implicated in *APOBEC3A* regulation (Oh *et al*, 2021; Isozaki *et al*, 2023), and WDR5 binding was also observed at this region in differentiating NHEKs (Fig 4F, Appendix Fig S7A). Analysis of ChIP-seq data from keratinocytes (Kouwenhoven *et al*, 2015; Rubin *et al*, 2017; Bernstein *et al*, 2010; Ernst *et al*, 2011) revealed a dominant peak for active histone marks (H3K27Ac, H3K4Me1, and H3K4Me3) at the -33kb enhancer where GRHL3 binding was detected (Fig

4F). ChIP-seq data from monocytes (Nurminen *et al*, 2018; Bernstein *et al*, 2010; Novakovic *et al*, 2016; Dunham *et al*, 2012), which also express *APOBEC3A* (Peng *et al*, 2007; Chen *et al*, 2006; Koning *et al*, 2009) but not *GRHL3* (Kudryavtseva *et al*, 2003), revealed a different profile, with abundant H3K27 acetylation and H3K4 methylation marking the -4kb promoter and a second predicted enhancer at -15kb but not at the -33kb enhancer (Figure 4F). Differential enhancer usage in keratinocytes and monocytes may explain the requirement for GHRL3 in the former but not the latter. GRHL3 and WDR5 binding to a region of the *ELF3* promoter containing three putative GRHL3 binding motifs was also evident (Appendix Fig S7B) but no peaks were observed at *IVL* promoter.

The relationship between *GRHL3* and *APOBEC3A* was further investigated in a dataset of 77,969 cells from healthy human airways (Deprez *et al*, 2020). Both *GRHL3* and *APOBEC3A* were predominantly (865/1545 (56%) of *GHRL3*-expressing cells and 230/623 (37%) of *APOBEC3A*-expressing cells) expressed in secretory epithelial cells of the nasal cavity which also expressed the differentiation markers *KRT10*, *IVL* and *ELF3* (Fig 4G). *APOBEC3B, MKI67* and *TOP2A* were predominantly expressed in cycling basal cells and suprabasal cells, again consistent with our observations from tonsil epithelium (Fig EV1). As expected, *APOBEC3A* was also expressed in monocytes and macrophages (9.8% and 9.5% of *APOBEC3A*-expressing cells respectively), while *GRHL3* was not (Figure 4G). Together, these data from tissues and cultured cells identify GRHL3 as a key transcription factor that acts to upregulate *APOBEC3A* expression during keratinocyte differentiation.

Although no single transcription factor activity displayed a consistently strong correlation with *APOBEC3B* expression (Dataset EV2), possibly due to the lower number of *APOBEC3B*-expressing cells in several of the datasets), correlations with E2F family transcription factors

are consistent with previous reports linking repressive E2F-containing complexes to *APOBEC3B* regulation (Periyasamy *et al*, 2017; Roelofs *et al*, 2020), and with its expression in proliferating cells.

Evidence for regulation of *APOBEC3A* by GRHL3 in SCC tissues and cell lines.

Having determined that *APOBEC3A* is expressed during the terminal differentiation of non-cancerous epithelial cells in the tonsil and oesophagus, and that this expression pattern could be recapitulated in immortalised but non-transformed epidermal keratinocytes in culture, we next investigated *APOBEC3A* and *APOBEC3B* expression patterns in scRNA-seq data from tumour samples. After inferring copy number variation (CNV) profiles for each cell by averaging gene expression levels over large genomic regions (Patel *et al*, 2014) (see methods for details), we identified 695 epithelial cells from our tumour samples with inferred CNV profiles that closely resembled those of cells from our matched normal tonsil cells (Appendix Figure S8). These were classed as non-malignant and further analyses were based on the 18,619 malignant epithelial cells remaining. Pathway analysis of the top 100 genes co-expressed with either *APOBEC3A* or *APOBEC3B* in the 18,619 malignant tumour cells from the 10 Southampton HNSCCs (7 of which were patient-matched with the healthy tonsil samples analysed in Figure 2 (Tables EV1, EV2)) and in the additional published scRNA-seq datasets from HNSCC(Puram *et al*, 2023; Kürten *et al*, 2021) and ESCC(Zhang *et al*, 2021) revealed similar results to those obtained when performing the analysis on data from healthy tonsil; *APOBEC3A* was again co-expressed with genes in pathways related to keratinocyte differentiation, while *APOBEC3B* was co-expressed with genes in pathways linked to cell division (Appendix Figure S9A-D and Datasets EV3-EV6).

Although it was not possible to visualise the four phenotypes (basal, proliferating, differentiating and terminally differentiated) on UMAPs due to the cells from individual tumours clustering by patient rather than by phenotype (Appendix Figure S9E), we again observed *APOBEC3A* co-expression with markers of differentiation and components of the RIPK4 pathway and *APOBEC3B* co-expression with markers of proliferation (Appendix Figure S10A). When analysing each of the 10 tumour samples in the Southampton HNSCC dataset individually, the same trends were observed in almost all cases (Appendix Figure S10B-K). SCENIC analysis of the four SCC datasets implicated GRHL3 as a potential regulator of *APOBEC3A* in squamous cell carcinoma as well as in healthy epithelia, with strong correlations between GRHL3 activity and *APOBEC3A* expression evident across all studies (Figure 5A, Dataset EV2). Having observed strong correlations between *APOBE3CA* expression and *GRHL3* expression and predicted activity in single cell data from HNSCC and ESCC, we next sought to determine whether GRHL3 may be involved in regulating *APOBEC3A* expression cancer arising in other tissues. Since too few tumour cells in the scRNA-seq datasets from lung, breast and urothelial cancer that we analysed (Table EV1) expressed *APOBEC3A* to permit co-expression analysis, we examined *APOBEC3A* expression (Fig EV2A), GRHL3 expression (Fig EV2B) and GRHL3 activity (Fig EV2C) in bulk RNA-seq data from The Cancer Genome Atlas (TCGA). Squamous cell carcinomas (notably of the head and neck (HNSC), cervix (CESC-SQ), oesophagus (ESCA-SQ), lung (LUSC), and bladder (BLCA) were among the cancers with highest *APOBEC3A* expression (Figure EV2A), and these also displayed the highest GRHL3 expression (Figure EV2B) and activity scores (as inferred from the expression of genes in the GRHL3 regulon identified in our earlier SCENIC analysis, Fig EV2C). As previously reported (Green *et al*, 2017), *APOBEC3A* was also highly expressed in acute myeloid leukaemia (LAML) but *GRHL3* was not, which is consistent with our earlier

conclusion that *APOBEC3A* is differentially regulated in keratinocytes and myeloid cells. We also observed strong correlations between *APOBEC3A* and *GRHL3* expression (Fig EV2D), and GRHL3 activity scores (Fig EV2E) in bulk RNA-seq data from SCCs, and from adenocarcinomas of the cervix (CESC-AD) and oesophagus (ESCA-AD). Other cancer types in which *APOBEC3A* has been implicated in somatic mutagenesis, such as breast cancer, lung adenocarcinoma and bladder cancer displayed weaker but nonetheless significant correlations between *APOBEC3A* expression and *GRHL3* expression and/or transcriptional activity, suggesting GRHL3 may play a role in promoting *APOBEC3A* expression in these tumours. It is important to note the limitations of performing this analysis in bulk RNA-seq data, in which *APOBEC3A* expression in cell types (e.g. tumour-resident macrophages or infiltrating neutrophils) that do not express GRHL3 will influence these correlations. Given the strong evidence from both single cell and bulk RNA-seq data that implicates GRHL3 in *APOBEC3A* regulation in HNSCC, we next analysed RNA-seq data from the 34 HNSCC cell lines in the Cancer Cell Line Encyclopaedia (CCLE) (Ghandi *et al*, 2019), observing correlations between *APOBEC3A*, *GRHL3* and differentiation-related genes, and inverse correlations between APOBEC3A and proliferation markers, *MKI67*, *MCM7* and *TOP2A* (Figure EV3A). Among those cell lines profiled by the CCLE, *APOBEC3A* and *GRHL3* mRNA levels were highest in BICR6 and BICR22; lines derived from an SCC of the hypopharynx and from a lymph node metastasis from a tongue SCC respectively (Edington *et al*, 1995) (Figure EV3B). *APOBEC3A* and *GRHL3* mRNA levels were higher in sub-confluent cultures of both BICR6 and BICR22 than in NIKS harvested under the same conditions (Appendix Figure S11) and we observed a significant reduction in *APOBEC3A* expression upon *GRHL3* knockdown in both cell lines (Figure 5B).

To gain further insight into the heterogeneity of *APOBEC3A* and *APOBEC3B* expression in HNSCC, we next analysed spatial transcriptomics data obtained from tissue sections representing the same cases as those from which our scRNA-seq were derived. Consistent with what we observed in the scRNA-seq analysis, *APOBEC3A* was expressed in regions that displayed high predicted GRHL3 activity (the GRHL3 target genes that comprise the GRHL3 module are listed in Table EV5) and expression of additional genes related to keratinocyte differentiation, while *APOBEC3B* was expressed in regions marked by high expression of proliferation markers (Figure 5C). Pathway analysis of genes co-expressed with *APOBEC3A* or *APOBEC3B* yielded similar results to those obtained from the scRNA-seq data but in addition to pathways associated with keratinocyte differentiation, the wound healing response (another process in which GRHL3 plays a critical role) was also overrepresented among those genes co-expressed with *APOBEC3A* (Table EV6, Appendix Figure S12). Since the Visium platform typically provides resolution of approximately 10 cells / spot depending on cell size and cellularity, we performed spot deconvolution, observing that the *APOBEC3A* reads from each spot were largely derived from epithelial (tumour) cells with expression also evident in monocytes and neutrophils, consistent with previous reports (Suspène *et al*, 2011; Aynaud *et al*, 2012; Chen *et al*, 2006). *APOBEC3B* reads were largely derived from the tumour cells (Appendix Figure S13). A representative example tumour section (case HN485), displaying regions of *APOBEC3A* expression with high GRHL3 activity ('GRHL3 module', composed of SCENIC-predicted target genes including *ELF3*) is shown in Figure 5d. In the same section, distinct *MKI-67*-positive regions of the tumour show peak expression of *APOBEC3B*. Strong *CDKN2A* expression (the gene encoding $p16^{INK4A}$, a biomarker for HPV-positive HNSCC) is evident throughout most of the tumour cells. GRHL3 activity and *APOBEC3A* expression were frequently highest near to the tumour surface.

Analysis of APOBEC3 protein expression in tissue samples has been hampered by a lack of suitable antibodies for detection by immunohistochemistry but we (M.A.C and R.S.H) recently developed a monoclonal antibody that specifically detects APOBEC3A in formalin-fixed, paraffin-embedded tissues (Naumann *et al*, 2023). Having confirmed specificity by staining of paraffin-embedded blocks generated from PMA-treated wild-type control and *APOBEC3A*-knockout (KO) NIKS (Figure S14), we conducted APOBEC3A immunohistochemistry on a tissue microarray (TMA) representing 20 HNSCC cases (10 HPV+ve and 10 HPV-ve). As predicted from our scRNA-seq and spatial transcriptomics data, some tumours were devoid of APOBEC3A, while others displayed abundant staining in more differentiated tumour cells, including in those cells surrounding keratin pearls – a distinguishing feature of well differentiated SCC (Figure EV4(I), left panel). Staining the same TMA with an antibody that binds to APOBEC3A, APOBEC3B and APOBEC3G (Brown *et al*, 2019) revealed characteristic nuclear APOBEC3B expression in tumour cells (Figure EV4, right panels). As expected, this was particularly evident in HPV-positive cases (Figure EV4 (II, III), right panels), in which APOBEC3B is upregulated by the viral E6 and E7 proteins (Vieira *et al*, 2014; Warren *et al*, 2015; Periyasamy *et al*, 2017; Mori *et al*, 2017). APOBEC3G is known to be expressed in the cytoplasm of T-lymphocytes and was evident in resident lymphocytes (e.g. Figure S12b(I) arrowheads). The pan-cellular staining of keratinizing cells with the APOBEC3A/B/G antibody is consistent with the APOBEC3A-specific staining (compare Figure EV4(I) boxed areas and EV4(III) insets between left and right panels). We also stained three cases (HN485, Figure 5E), HN482 and HN494 (Appendix Figure S15), for which we had also generated spatial transcriptomics data, observing good concordance between the patterns of mRNA and protein positivity for both *APOBEC3A* and *APOBEC3B*

409 (compare Figure 5D and E and Appendix Figure S13A and B). Importantly, in addition to
410 providing further validation of the specificity of our antibodies, these data confirm that our
411 conclusions relating to *APOBEC3A* and *APOBEC3B* expression drawn from mRNA data
412 (scRNA-seq, spatial transcriptomics) are valid at the protein level.
413
414 Finally, while *APOBEC3A* expression was largely confined to IVL^{+ve} / $MKI67^{-ve}$ (non-cycling)
415 tumour cells, the correlation between *APOBEC3A* and *IVL* expression was weaker in the SCC
416 datasets than in the normal tonsil epithelial cells, and in the UMAPs from the Southampton
417 HNSCC dataset, *APOBEC3A* expression was apparent in IVL^{-ve} cells, which also displayed high
418 predicted GRHL3 activity (Figure 5A). This was most obvious in two tumours (HN489 and
419 HN492; compare Figure 5A and Figure S9E), suggesting that under certain conditions,
420 activation of GRHL3 may induce *APOBEC3A* in cycling tumour cells. Given the considerable
421 evidence linking APOBEC3A-mediated mutagenesis to deamination of the lagging strand
422 during DNA replication (Green *et al*, 2016; Haradhvala *et al*, 2016; Hoopes *et al*, 2016;
423 Morganella *et al*, 2016; Seplyarskiy *et al*, 2016; Stewart *et al*, 2020), we used gene
424 expression data to assign cells from our normal tonsil and HNSCC datasets to G0/G1, S, or
425 G2/M phase of the cell cycle (Figure 5F inset) and compared *APOBEC3A* expression and
426 GRHL3 activity in those cells predicted to be in S-phase. While as expected, the majority of
427 S-phase cells did not express *APOBEC3A*, considering all S-phase cells in which *APOBEC3A*
428 expression was detectable (more than zero reads) we observed a small minority that
429 expressed considerably more *APOBEC3A* mRNA than was seen in S-phase cells from normal
430 tonsil epithelium (Figure 5F; black dots on the boxplot represent cells that are statistical
431 outliers with respect to the level of *APOBEC3A* found in normal tonsil). The S-phase tumour
432 cells with high *APOBEC3A* expression were all designated a binary GRHL3 activity score of

'on', suggesting that GRHL3 can drive *APOBEC3A* expression in tumour cells undergoing DNA replication, potentially causing APOBEC3A-mediated mutagenesis. The fact that we only observed high *APOBEC3A* expression in a small minority of S-phase cells in our HNSCC samples is consistent with the proposed episodic nature of APOBEC-mediated mutagenesis, in which the chances of observing a mutagenic burst in the snapshot provided by a tumour biopsy are low (Petljak *et al*, 2019, 2022a, 2022b; Smith & Fenton, 2019).

Discussion

Our analysis of *APOBEC3A* and *APOBEC3B* gene expression in healthy and cancerous squamous epithelia provides new insight into how these genes are regulated and raises several questions that warrant further investigation. The low expression of *APOBEC3B* in normal epithelium and increased levels in tumours that we observed in scRNA-seq datasets is consistent with previous analyses of bulk tissue samples and breast cancer cell lines (Burns *et al*, 2013a), in which repressive E2F/RB complexes have been shown to silence expression in quiescent cells (Periyasamy *et al*, 2017; Roelofs *et al*, 2023, 2020). Loss of p53-mediated repression of *APOBEC3B* transcription, resulting either from *TP53* mutation (observed at high frequency in HPV-negative HNSCC and ESCC) or from HPV E6/E7 activity in HPV-positive HNSCC (Vieira *et al*, 2014; Periyasamy *et al*, 2017) is also likely an important driver of *APOBEC3B* expression seen in many of the SCC samples we analysed.

The high expression of *APOBEC3A* in tonsil and oesophageal epithelium could indicate a role in defence against one or more viruses with tropism for the upper aerodigestive tract. Wild-type adeno-associated virus (AAV, a target for APOBEC3A (Chen *et al*, 2006)) infects keratinocytes via binding to heparan sulphate proteoglycans and AAV genomic DNA has

457 been isolated from tonsils (Schnepp *et al*, 2005). *APOBEC3A* and *APOBEC3B* have both been
458 implicated in host responses to HPV infection (Wang *et al*, 2014; Vartanian *et al*, 2008;
459 Vieira *et al*, 2014; Warren *et al*, 2015) and although our data suggest that neither are
460 expressed in quiescent basal cells of the tonsil epithelium (the target cell for HPV infection),
461 *APOBEC3B* is expressed in those cells undergoing division in the parabasal layer, while
462 *APOBEC3A* is expressed in cells undergoing terminal differentiation; a pattern also evident in
463 an area of normal stratified epithelium at the margin of an HPV-associated oropharyngeal
464 SCC in which *APOBEC3A* and *APOBEC3B* were detected by RNA *in situ* hybridization (Kono *et*
465 *al*, 2020). Both genes are therefore expressed (at least in the absence of infection) under
466 cellular conditions in which different stages of the HPV productive life cycle occur: genome
467 maintenance following E6/E7-induced cell cycle entry in the basal / para-basal layer and
468 genome amplification in terminally differentiating cells (Doorbar *et al*, 2012). Whether this
469 pattern of APOBEC3 gene expression represents a host adaptation to papillomaviruses, or to
470 other pathogens that infect the upper-aerodigestive tract remains to be determined.
471 Alternatively, the expression of *APOBEC3B* in dividing keratinocytes and *APOBEC3A* during
472 terminal differentiation may reflect hitherto unidentified physiological roles related to these
473 processes. *APOBEC3B* is also expressed as breast cancer cell lines approach mitosis and its
474 knockdown slows proliferation, suggesting a role in cell cycle progression that might be
475 linked to its function as a transcriptional co-activator for the oestrogen receptor
476 (Periyasamy *et al*, 2015; Roelofs *et al*, 2023). Unlike in normal breast epithelium (Figure 1) or
477 in MCF10A, a cell line derived from normal mammary epithelium (Roelofs *et al*, 2023), we
478 observed sufficient *APOBEC3B* expression in our scRNA-seq data from normal tonsil
479 epithelium and from NIKS (Figure 3e) to observe a clear enrichment in G2/M-phase cells,
480 suggesting APOBEC3B may play a role in normal keratinocytes entering cell division.

APOBEC3B expression in G2/M-phase is not unique to epithelial cells either; it has also been documented in myeloma cells and in B-cells from healthy bone marrow (Hirabayashi *et al*, 2021). *APOBEC3A* induction during Ca^{2+}induced keratinocyte differentiation has been linked to hypermutation of mitochondrial DNA (Wakae *et al*, 2018), although the functional significance of this remains unclear. More investigation of *APOBEC3A* and *APOBEC3B* function in epithelial cells is required but it is maybe not surprising that by restricting *APOBEC3A* expression to post-mitotic keratinocytes and *APOBEC3B* expression to the G2/M phase of proliferating cells, mechanisms have evolved to restrict these potentially dangerous deaminases to contexts in which DNA replication is not occurring.

The identification of GRHL3 as a transcription factor responsible for driving *APOBEC3A* expression in differentiating keratinocytes and in squamous cell carcinoma highlights the power of single cell transcriptomics to uncover gene regulatory networks. In this case using SCENIC (Aibar *et al*, 2017) we observed striking correlations between GRHL3 activity scores and *APOBEC3A* expression across multiple scRNA-seq datasets from healthy and cancerous epithelia and validated the prediction using RNA interference in cultured cells. GRHL3 is a key transcription factor in epidermal keratinocytes, required not only during differentiation but also in migration during developmental processes and in wound healing (Ting *et al*, 2005; Caddy *et al*, 2010; Hislop *et al*, 2008; Gordon *et al*, 2014; Yu *et al*, 2006, 2008). Given the extensive overlap between the molecular processes that are active during wound healing and cancer (MacCarthy-Morrogh & Martin, 2020), this latter function may be of particular relevance to driving *APOBEC3A* expression in tumour cells, including in those undergoing DNA replication and warrants further investigation.

While most studies have focused on its function in the epidermis, *GRHL3* and its murine orthologue, *Grhl3*, have been implicated as suppressors of squamous carcinogenesis in the mucosal epithelia of the oral cavity and oesophagus as well as in skin (Darido *et al*, 2011; Georgy *et al*, 2023). *GRHL3* loss-of-function mutations have not been reported in SCC but it is located at a locus (1p36.11) that is frequently deleted in HNSCC and it is also targeted by a micro-RNA (miR-21) that is over-expressed in HNSCC. Accordingly, *GRHL3* expression in SCCs was demonstrated to be significantly lower than in adjacent normal tissue(Georgy *et al*, 2015; Darido *et al*, 2011). Our scRNA-seq analysis of normal tonsil and HNSCC cases is agreement with the above studies; we observed higher mean *APOBEC3A* expression in normal tonsil epithelial cells than in tumour cells from patient-matched HNSCC cases (Figure 1). Similarly, while spatial transcriptomics and immunohistochemistry of sections from these HNSCCs revealed widespread *APOBEC3B* expression (particularly in HPV +ve cases, as expected), *APOBEC3A* was not expressed in all cases and in those tumours where expression was observed, it was restricted to areas of high GRHL3 activity (Figure 5). Repression of *APOBEC3B* expression by the E2F4/RB-containing DREAM (dimerization partner, RB-like, E2F and MuvB) complex has been reported (Periyasamy *et al*, 2017), which may explain its confinement to proliferating cells in healthy squamous epithelia. The absence of *APOBEC3A* in basal and terminally differentiated cells suggests it too is subject to transcriptional repression; another mode of regulation that if disrupted could enable bursts of mutagenic APOBEC activity in cancer cells.

These observations, together with our siRNA experiments in HNSCC cell lines, suggest that in SCC at least, *APOBEC3A* expression is confined to the minority of tumour cells in which *GRHL3* is expressed and active. If we consider that APOBEC activity is only likely to be

mutagenic in cycling cells (or in cells that have re-entered the cell cycle without repairing deaminated cytosines), the pool of tumour cells at risk of APOBEC3A-mediated mutagenesis is likely limited to those rare cells highlighted in Figure 5f, in which *APOBEC3A* expression coincides with DNA replication. It follows that if such *APOBEC3A*-expressing tumour cells were to acquire mutations that caused them to become more proliferative (as might be expected if the subclone were to expand to constitute a significant portion of the tumour) this would result in loss of *APOBEC3A* expression (and potentially an increase in *APOBEC3B* expression). This model could explain the somewhat puzzling observation that tumours with strong enrichment for mutational signatures (YpTp[C>T/C>G]pN) associated most strongly with APOBEC3A often express very low levels of *APOBEC3A*, while *APOBEC3B* expression is more closely correlated with enrichment for the APOBEC mutational signatures but appears to be responsible for generating a smaller fraction of these mutations(Chan *et al*, 2015; Jalili *et al*, 2020; Petljak *et al*, 2022a; Carpenter *et al*, 2023).

Finally, we note that activation of GRHL3 in keratinocytes plays a key role in resolving psoriatic lesions by suppressing inflammatory mediators and driving epidermal repair (Shi *et al*, 2021; Gordon *et al*, 2014). Our finding that GRHL3 regulates *APOBEC3A*, which was originally discovered as a protein (Phorbolin-1) that is highly upregulated in psoriatic lesions (Rasmussen & Celis, 1993; Madsen *et al*, 1999) finally provides a potential mechanistic explanation for this early observation that predated mapping of the *APOBEC3A* gene (Jarmuz *et al*, 2002) by almost a decade.

Methods

Ethics / patient samples

553 Patients undergoing biopsies of suspected primary Head and Neck cancers at University
554 Hospitals Dorset (UHD) NHS Foundation Trust were consented to take part in a study; "Head
555 and Neck cancer: molecular, cellular and immunological mechanisms". This study is NIHR
556 portfolio adopted (portfolio No. 8130) and has been approved by the National research
557 ethics service South Central committee (reference No. 09/H0501/90). Tumour samples from
558 ten oropharyngeal patients (Table EV1), as well as normal tissue samples from the
559 contralateral tonsil for seven of the patients (collected at the time of diagnostic biopsy)
560 were selected for single cell RNA sequencing. Informed consent was obtained from all
561 subjects and the experiments conformed to the principles set out in the WMA Declaration
562 of Helsinki and the Department of Health and Human Services Belmont Report. Sample
563 number (17), including 10 tumour samples and 7 matched tumour-free contralateral tonsil
564 controls, was dictated by sample availability and funding as opposed to statistical
565 considerations.
566
567 *Single cell suspension preparation*
568 Upon receipt, tissue samples were washed once in Dulbecco's modified eagle medium
569 (Sigma #D5671) containing 10% Foetal Calf Serum, 1% Penicillin/streptomycin, 1% L-
570 Glutamine, 1% Amphotericin, 1% Sodium pyruvate, and 12.5mM HEPES. Samples were
571 chopped into 1-2mm size pieces prior to enzymatic digestion. The first stage of the
572 enzymatic digestion was performed using Liberase^{TM} (Sigma #5401020001) at 100µg.mL^{-1}
573 and DNase-1 (Sigma #DN25) at 16 units.mL^{-1} in cDMEM. The solution was sterile filtered
574 using a 0.22µm syringe filter and the sample material was suspended in up to 5mL of
575 cDMEM/Liberase solution. Samples were then sealed and placed in a benchtop
576 shaker/incubator at 37^{O}C and 150rpm for fifteen minutes and then removed. The tube was

left to stand until the undigested material had settled to the bottom then the upper 4 – 4.5mL was carefully transferred to a fresh tube, the Liberase fraction. For the second digest (Col+) cDMEM containing collagenase-P (Sigma #11213857001) at 3 units.ml^{-1}, liberase at 100µg.mL^{-1}, dispase (Sigma #D4693) at 0.5 units.mL^{-1}, elastase (Sigma #E1250) at 400µg.mL^{-1}, trypsin (Sigma #T4799) at a final concentration of 0.25%, and DNase-1 (16 units.mL^{-1}) was added to the remaining material through a 0. 22µm sterile syringe filter. The Col+ digest was returned to the incubator (37^{O}C / 150rpm) for up to a maximum of 45 minutes (or until digestion is complete) with trituration performed using a 5mL graduated pipette every 15 minutes. After 45 minutes the Col+ fraction was removed from the incubator and any remaining undigested pieces were allowed to settle at the bottom of the tube; the supernatant was then transferred to a fresh sterile tube. Any remaining tissue was set aside.

The post digestion process was the same for both the Liberase and Col+ fractions. Complete DMEM, up to 10 mL, was added to each fraction and both cell suspensions were pelleted at 350rcf for 5 minutes. Supernatant was removed and RBC lysis buffer (Biolegend #420301) used to remove erythrocytes for 10 minutes at 4^{O}C. The samples were then washed in PBS and suspended in residual volume and then held at 4^{O}C until the Col+ fraction was prepared. Cell pellets were suspended in PBS containing 2% BSA-Fraction V (Scientific Lab Supplies #10735108001) and passed through a pre-wetted 40µm filter. Both samples were then counted and viability assessed by Trypan blue exclusion. A final visual check of sample quality was also performed to ensure there were no large clumps of cells nor debris from the digestion. Finally the two fractions were used to make a 100µL suspension of 100,000 cells of which 10,000 were from the liberase fraction and 90,000 from the Col+ fraction, and

2% BSA in PBS was used as the diluent. This cell suspension was then run immediately on a Chromium Controller (10X Genomics).

Fluorescence-activated cell sorting

Flow cytometry to determine the proportions of cell types in the disaggregated samples was carried out using a FACSCanto II (BD Biosciences). Cell viability was assessed using Zombie Violet™ (Biolegend #423114). The following antibodies were purchased from Biolegend: EpCAM (#369806), CD90 (#328114), CD45 (#368508), CD31 (#303118), CD3 (#300426). A minimum of 20,000 events were acquired for each case. Gating was applied to exclude debris, dead cells, doublets and the immune compartment (CD45+ and/or CD3+) before enumerating the numbers of endothelial, epithelial, and CD90 positive fibroblasts in the sample.

Single cell RNA sequencing

Five thousand single cells from each sample were captured on a Chromium Controller™ (10X Genomics) system using Illumina single cell 3' gene expression and library preparation kits (V3.1 #1000269). Sample capture, sample indexing, and library preparation were carried out strictly according to manufacturer's instructions. Size distribution, quality control, and quantification of the libraries was assessed using High Sensitivity DNA chips (Agilent Technologies #5067-4626) and KAPA library quantification qPCR kit (Roche #07960140001). Prepared libraries were pooled and sent to Oxford Genomics (UK) for 150-base pair, paired-end sequencing on a Novaseq6000™.

Sequence alignment and annotation

Cell Ranger (10x Genomics) pipelines (mkfastq, count) were used to align reads, filter, count barcodes and UMIs (unique molecular identifiers) and generate feature-barcode matrices. FASTQ files were aligned to the Human reference genome (GRCh38–2020-A) which had the HPV genome concatenated to both FASTA and GTF reference files. HPV reference sequences were downloaded from PaVE: The Papillomavirus Episteme (https://pave.niaid.nih.gov). The HPV-16 reference sequence (NC_001526) was used in the first instance and in cases requiring further identification of the HPV subtype references including HPV-33 (OQ_672679) and HPV-18 (NC_001357) were also created. In all cases the individual HPV ORFs were identified in the FASTA and GTF files to allow identification during alignment.

Pre-processing of scRNA-seq data

For each sample, raw gene expression matrices were integrated into one dataset using Seurat package (v4.0.1). The resulting feature-barcode matrix from the cell ranger pipeline was transformed into a Seurat object with patient metadata. Cells with less than 200 expressed genes were removed. Genes expressed in less than 3 cells were also filtered out. Further low-quality cells were removed based on mitochondrial gene percentage with the threshold for calculated as the median + 3*median absolute deviation. Cells above the threshold were removed ensuring high quality cells remained.

Normalisation and integration

After quality control steps, the data was normalised to adjust for differences in sequencing depth between samples. sctransform was chosen to normalise and variance stabilize the count data109. Reciprocal PCA ('RPCA') Seurat integration workflows were utilised for integration. The Seurat object was first split by patient into a list of 10 smaller objects, in

which each dataset was normalised by sctransfrom individually. 3000 features were selected via 'SelectIntegrationFeatures' function. 'PrepSCTIntegration' was run prior to anchor identification to ensure sctransfrom residuals from the 3000 features identified (by SelectIntegrationFeatures) were present. Anchors, used to integrate objects, were found between datasets using FindIntegrationAnchors, with the normalization.method set to 'SCT' and reduction set to 'rpca' (all other parameters were default). Finally, IntegrateData was run, again specifying 'SCT' as normalization.method. This integration pipeline was run using IRIDIS High Performance Computing Facility (University of Southampton).

Dimensionality reduction, visualisation, and clustering

Principal component analysis (PCA) was used to reduce the dimensionality of the datasets. Principal components were assessed by JackStraw and elbow plots to select an appropriate number of dimensions to be used downstream. Dimensions 1:30 were selected in the following steps. Clustering was performed in Seurat, which constructs a k-nearest neighbours graph and refines this using the shared local neighbourhood overlap between cells ('FindNeighbours'; 'FindClusters'). RunUMAP command was used to visualise the data in a UMAP (Uniform, Manifold, Approximation and Projection) plot.

Identification of marker genes and cell type identification

After clustering and UMAP projection, broad cell populations were identified based on expression of known marker genes e.g., PTPRC/CD45+ immune cells, LUM+ Fibroblasts, RGS5+ Mural cells, PECAM1/CD31+ endothelial cells. Epithelial cell clusters were identified based on the expression of EPCAM, SFN and cytokeratin genes (e.g., KRT14, KRT17, KRT6A, KRT5, KRT19) – with absence of expression of other cell-type markers. Epithelial cell clusters

were then subset into a separate object, with new variable features found by re-running sctransform, PCA and clustering, whereby any clusters suggestive of doublets were removed based on the expression of non-epithelial markers (identified using FindAllMarkers) and examining UMI/feature number. The remaining epithelial cells were then used for further analysis.

Unsupervised clustering of epithelial cells

A total of 22,595 epithelial cells were subset into tumour (19,314 cells) and normal (3,281 cells) Seurat objects. The normal epithelial cells underwent further quality control, 658 cells were removed as suspected doublets due to high expression of immune cell and fibroblast related genes. The remaining 2,649 cells were clustered using the first seven principal components with a resolution of 0.2, and a k parameter of 30. Cell subtypes were identified using known gene markers for epithelial and keratinocyte cell states, and *a priori* knowledge. The density of *APOBEC3A* and *APOBEC3B* expression was visualised on UMAPs using the Nebulosa R package (v1.9.0). R package inferCNV (v1.3.3) was used to identify malignant and non-malignant cells. The epithelial cells from our matched normal tonsil samples (grouped by differentiation status: basal; proliferating; differentiating and terminally differentiated) were used as reference cells, and the infercnv::run function was used with a cutoff of 0.1 and HMM=FALSE, and clustered by patient (Appendix Figure S8A). An inferCNV score (number of genes with inferred CNV / total number of genes) was calculated for each cell. The higher the score, the more likely a cell was malignant. The distribution of inferCNV scores was clearly bimodal, enabling us to set a threshold for malignant cells at the lowest point between the two distributions (0.12, Appendix Fig S8B). This resulted in 695 non-malignant cells that were removed from our analyses of gene

expression in tumour cells and 18,619 malignant cells that formed our tumour cell dataset. The tumour cells were clustered using the first 15 principal components with a resolution of 0.2 and k parameter of 60.

Gene co-expression

The COTAN R package (v2.0.1) was used to investigate the co-expression of gene pairs for scRNA-seq datasets. For both *APOBEC3A* and *APOBEC3B*, the top 100 genes with a positive correlation index were identified and used in pathway analysis using the enrichR package (v3.2) and GO biological processes gene sets. Relevant epithelial differentiation and proliferation markers were chosen and *APOBEC3A*/*APOBEC3B* co-expression values with selected genes were plot in heatmaps using R package pheatmap (v.1.0.12).

SCENIC analysis

Transcription factor (TF) analysis of scRNA-seq data was performed using pySCENIC (v0.12.1) (Kumar *et al*, 2021) and motif collection version mc9nr. TF activity AUC score for each cell was overlaid on UMAPs for visualisation and the score was correlated with *APOBEC3A* and *APOBEC3B* expression using Spearman correlation and corrected for multiple tests using Benjamini-Hochberg. Binary activity (on/off) of each TF was determined based on a threshold generated by pySCENIC and each cell was classified as on (1) or off (0). The *APOBEC3A* levels in 'GRHL3 on' and 'GRHL3 off' cells were compared using Wilcoxon rank sum test. Four groups of *APOBEC3A*/*GRHL3* expression were considered: *APOBEC3A*$^{-}$/*GRHL3*$^{-}$, *APOBEC3A*$^{+}$/*GRHL3*$^{-}$, *APOBEC3A*$^{-}$/*GRHL3*$^{+}$, and *APOBEC3A*$^{+}$/*GRHL3*$^{+}$. The number of cells in each group were counted and a comparison between the number of '*GRHL3* on' (*GRHL3*$^{+}$) cells that were also *APOBEC3A*$^{+}$ were compared with the number of '*GRHL3* off'

(*GRHL3*$^{-}$) cells that were *APOBEC3A*$^{+}$ using Fisher's exact test. The FindAllMarkers function in Seurat R package was used to perform the differential transcription factor activity analysis, using a threshold fold change of 1.1 and Benjamini-Hochberg adjusted P of 0.05.

GHRL3 binding motif analysis

Homer (v4.11) function findMotifsGenome with mismatches threshold set to 2 was used to identify the frequency of GRHL3 binding motifs in differentiating NHEK ChIP-seq for GRHL3 peaks. The three binding motifs searched for were based on previous literature: AACCGGTT (Boglev *et al*, 2011), AACCTGTT and AACAGGTT (Yu *et al*, 2006). The percentage of times each base was located at each position in the binding motif was calculated and visualised using R package motifStack (v1.44.1) and dependencies. GRHL3 and WDR5 ChIP-seq for differentiating and proliferating keratinocytes ChIP-seq data (bedfiles), and monocyte and keratinocyte H3K27Ac, H3K4Me1 and H3K4Me3 ChIP-seq data (BigWig files) was obtained from CistromeDB and visualised in the UCSC genome browser.

Airways single cell atlas analysis

Publicly available data for healthy human airways (HG38 version) was obtained from https://doi.org/10.1164/rccm.201911-2199OC. Only cells expressing *APOBEC3A* (623 cells), *APOBEC3B* (1,008), *GRHL3* (1,545), *ELF3* (45,597), *IVL* (113), *KRT10* (52,987), *MKI67* (730), and *TOP2A* (1,060) were considered for individual analysis. Proportions of each cell type that a gene was expressed in was calculated and visualised in stacked bar plots.

Spatial transcriptomic analysis

All steps leading up to sequencing (from the bench side) were performed per manufacturer recommendations on 6.5mm capture areas using the Visium V2 cytassist workflow. All the samples were run through the Spaceranger pipeline (v2.0.0) as per 10X Genomics/Visium guidelines.

Count matrices were loaded into Seurat. Samples were normalised using SCTransform function (using the variance-stabilizing transformation). To identify spot clusters across patients, samples were integrated using the Seurat v3 CCA anchor finding method (FindIntegrationAnchors and IntegrateData). The 3000 variable features selected for integration were then used for principal component analysis (PCA), followed by FindNeighbors and FindClusters for (shared) nearest-neighbor graph construction and cluster determination respectively. Uniform manifold approximation and projection (UMAP) algorithm (1:20 dimensions) was used to visualise the batch corrected integrated dataset. Resulting clusters were inspected, with poor quality clusters removed. The GRHL3 module score for each spot was calculated using AddModuleScore with 127 genes identified by SCENIC as potential target genes for GRHL3 binding in normal epithelium and HNSCC. Spatial feature expression plots were generated with the SpatialFeaturePlot function in Seurat.

Robust Cell Type Decomposition (RCTD) with spacexr 2.2.1111 in R was used to deconvolve Visium spots into cell types using the annotated scRNA-Seq HNSCC reference dataset. RCTD was ran with default parameters and doublet mode set to ‘full’ on each individual patient sample, with resulting deconvoluted normalised weights for each cell type obtained.

APOBEC3A expression in cancer cell lines

Expression data for 34 head and neck cancer cell lines from the Cancer Cell Line Encyclopaedia (CCLE) (Barretina *et al*, 2012) was obtained from the resource CellminerCDB (Luna *et al*, 2021) for differentiation and proliferation marker genes, *APOBEC3A*, and genes in the RIPK4 pathway. Spearman correlation coefficients were calculated pairwise for all genes.

TCGA RNA-seq analysis

Data were collected from the UCSC Xena functional genomics browser [https://xenabrowser.net]. Batch corrected gene expression data (RNAseq, log2(normalised value + 1)) for 11,060 patients (version 2016-12-29), and clinical data for 12,591 patients (version 2018-09-13) were downloaded for the TCGA pancancer (PANCAN) cohort (31 cancer types). Cervical (CESC) and oesophageal (ESCA) cancer cohorts were separated into squamous (CESC-SQ and ESCA-SQ) and adenocarcinoma (CESC-AD and ESCA-AD). *APOBEC3A* and *GRHL3* expression was visualised in boxplots made with R package ggplot2(v3.5.1) across all cancer types, sorting from highest median expression to the lowest. A GRHL3 signature was calculated for each sample by summing the means of the 127 genes predicted as being regulated by *GRHL3* in previously described SCENIC analysis. This score was visualised in boxplots for each cancer type.

Tissue microarrays

Tissue microarrays (TMAs) were constructed from paraffin-embedded HNSCC and normal oral mucosa (10 HPV+ve HNSCC, 10 HPV-ve HNSCC, 10 fibroepithelial polyps) using triplicate, randomly selected, 1-mm tumour cores (Aphelys Minicore 2, Mitogen,

Harpenden, UK). Automated immunostaining (DAKO/Agilent Autostainer) was performed in a CPA-accredited clinical cellular pathology department.

Immunohistochemistry

Staining of tissue microarrays and full-face sections was performed on a Dako link automated staining machine according to the manufacturer's instructions. The following antibodies were used: rabbit monoclonal anti-human APOBEC3A/B/G (Cell Signaling Technology, Cat#81001; 1:100 dilution with Dako FLEX TRS high pH retrieval); rabbit monoclonal anti-human APOBEC3A (UMN-13); 1:1000 dilution with Dako FLEX TRS high pH retrieval). Slides were scanned on an Olympus VS110 Digital Slide Scanner using a 20x magnification air objective. Staining and analysis of staining was performed blinded to the results of spatial transcriptomics profiling of adjacent sections.

Cell culture

Low-passage Normal immortalised keratinocytes (NIKS) and Normal primary human keratinocytes from pooled adult donors (Sigma C-12006) were cultured in FC medium (3:1 Ham's F12:DMEM, 5% foetal bovine serum (FBS), 10 ng/ml murine submaxillary gland EGF, 24 µg/ml adenine, 5 µg/ml insulin, 8.3 ng/ml cholera toxin, 0.4 µg/ml hydrocortisone, 1% penicillin/streptomycin) on a feeder layer of mitomycin C-treated mouse embryonic fibroblasts (3T3-J2). BICR6 and BICR22 cells were cultured in DMEM supplemented with 10% foetal bovine serum, 2 mM L-Glutamine, 0.4 µg/ml hydrocortisone and 1% penicillin/streptomycin. Cells were routinely checked and confirmed mycoplasma-negative by qPCR (Mycoplasmacheck, Eurofins Genomics) upon thawing and were subsequently used for experiments within 2-3 passages.

qRT-PCR

RNA purification was performed using the Monarch Total RNA Miniprep Kit (New England Biolabs) and on-column DNase digestion. cDNA was synthesised from RNA using LunaScript® Reverse Transcriptase (RT) SuperMix Kit (New England Biolabs). Gene-specific primers were synthesised by IDT and are shown in Table 1. The qRT-PCR primers for *APOBEC3A*, *APOBEC3B* and TATA binding protein (*TBP*) were published previously (Refsland *et al*, 2010) and the remaining qRT-PCR primers were designed using OriGene's qPCR primer design tool (https://www.origene.com). All real-time PCR reactions were performed using duplicate technical repeats on a QuantStudio Real-Time PCR system (Applied Biosystems) with amplification using PowerUp™ SYBR™ Green Master Mix for qPCR (Applied Biosystems). The thermal cycling conditions were at 50^{o}C for 2 min followed by an initial denaturation step at 95^{o}C for 10 min, 40 cycles at 95^{o}C for 15s and 60^{o}C for 1 min, followed by 95^{o}C for 1 min, 60^{o}C for 1 min and 95^{o}C for 1s. Standard curves for *APOBEC3A* and *APOBEC3B* were derived using plasmids pRH3097-A3A (R.S.H lab) and pCMV4-APOBEC3B (a kind gift from Prof Mike Malim, Kings College London, UK) respectively. Standards for all other qRT-PCR target genes were constructed by cloning PCR amplicons generated from a NIKS cDNA library into pCR™ Blunt II-TOPO™ using the Zero Blunt™ TOPO™ PCR cloning kit (Thermo Fisher) as per the manufacturer's instructions. PCR was conducted using the KAPA HiFi 2X MasterMix (Roche) according to the manufacturer's instructions with 10 ng input cDNA and for all target genes except *TBP* (for which additional primers are listed in Table 1), amplicons were generated using the qRT-PCR primers. All plasmids are available from the authors upon request.

siRNA transfections

Silencer Select small interfering RNAs (siRNA) were purchased from ThermoFisher Scientific (Negative control (NC#1) Cat No 4390843; GRHL3 (#1) Cat No s33753; GRHL3 (#2) Cat No s33754). NIKS were plated in 6-well plates at a density of 2 x 10^5 cells / well and BICR6, BICR22 at 1.5 x 10^5 cells / well, with 1 x 10^5 feeder cells / well and were transfected with 2 nM of siRNA using 2 uL of Lipofectamine RNAiMAX (ThermoFisher Scientific) per well according to the manufacturer's instructions (reverse transfection method). Transfection complexes were removed after 24h, followed by (NIKS) 48h recovery period and 24h treatment with 100 nM afatinib (Fisher Scientific #16463748) or removal of EGF and insulin and reduction to 0.5% FBS for 48h to induce differentiation, or 3h treatment with 100 ng/ml PMA (Stem Cell Technologies #74042). BICR6, BICR22 cells were allowed to recover for 42h post-transfection with a media change 18hr prior to cell collection.

APOBEC3A KO NIKS

APOBEC3A knockout NIKS clones were generated by using CRISPR-Cas9 to insert the sequence tagttagttag (to terminate translation in all three reading frames), followed by the bovine polyadenylation signal (bpA) at the end of exon 1, to generate an allele in which an mRNA encoding only the first 7 amino acids of APOBEC3A is produced (the gene targeting strategy is summarized in Appendix Figure S14A). Following the split nickase CRISPR method for increased specificity (Cong *et al*, 2013), single guide (sg)RNAs were designed by entering a 200 base-pair genomic sequence surrounding the *APOBEC3A* start codon into http://crispr.mit.edu/. Oligonucleotides (Integrated DNA Technologies) encoding the sgRNAs (Table 1) were annealed and cloned into pX335-U6-Chimeric_BB-CBh-hSpCas9n(D10A), a gift from Feng Zhang (Addgene plasmid # 42335; http://n2t.net/addgene:42335; RRID:Addgene_42335) using restriction enzyme Bbs I (NEB

as per the Zhang lab protocol (https://www.addgene.org/crispr/zhang/). A targeting construct was generated using NEBuilder® HiFi DNA assembly to combine 1kb 5' and 3' homology arms, the translation/transcription terminator sequence and a PGK-Puro-ΔTK cassette (Chen & Bradley, 2000) flanked by FRT sites into a pBluescript plasmid backbone (Appendix Figure S15A). The 5' homology arm contained point mutations at the CRISPR target site to prevent re-cutting following successful recombination into the locus. 5' and 3' homology arms were synthesized as g-blocks (Integrated DNA Technologies) and the pBluescript backbone and FRT-Puro-ΔTK-FRT cassette (a kind gift from Dr Su Kit Chew) were amplified by HiFi PCR using primers containing adapters for NEBuilder assembly. The targeting construct was verified by Sanger sequencing and co-transfected into NIKS, together with pX335 constructs containing the left and right sgRNAs using Fugene HD transfection reagent (Promega), as per the manufacturer's recommendations. Transfected NIKS were selected using puromycin (0.75 μg/ml) for 48 hours and following PCR genotyping to detect successful targeting, single cell clones were generated by plating NIKS at limiting dilution in 96 well plates, with each well containing $1x10^3$ mitomycin C-treated 3T3-J2 feeder cells. Feeder cells were replenished weekly as clones were expanded. Clones were screened by PCR genotyping to identify homozygous knockouts and transfected with GFP-Flippase (generated by cloning mouse codon-optimized Flippase (Flpo), a gift from Philippe Soriano (Addgene plasmid # 13792; http://n2t.net/addgene:13792; RRID:Addgene_13792) into pEGFP-N1 (Clontech)). Transfected cells were isolated by Fluorescence Activated Cell Sorting and PCR genotyping was conducted to confirm removal of the FRT-flanked PGK-Puro-ΔTK cassette. Loss of *APOBEC3A* expression and retention of *APOBEC3B*, *APOBEC3C* and *APOBEC3F* expression in knockout clones (C5, F6, and G6) was confirmed by reverse transcriptase PCR of PMA-stimulated NIKS (100 ng/ml / 24h) using the qRT-PCR primers

listed in Table 1 (Appendix Figure S15B). *APOBEC3D*, *APOBEC3G* and *APOBEC3H* were undetectable in wild-type or *APOBEC3A* KO NIKS by endpoint RT-PCR. To test the specificity of anti-APOBEC3A clone UMN-13 in immunohistochemistry, formalin-fixed, paraffin-embedded cell blocks were made by embedding wild-type and *APOBEC3A* KO (clone C5) NIKS cell pellets in agarose following 24h treatment with 100 ng/ml PMA).

DDOST RNA editing assay

DDOST editing at C558 was measured as described previously (Oh & Buisson, 2022) using 250 ng input RNA for cDNA synthesis. Digital PCR was conducted using the Absolute-Q instrument (ThermoFisher), with 1 uL of 1:4-diluted cDNA.

Statistical Analysis

Statistical analysis was performed using GraphPad Prism for qRT-PCR and digital PCR experiments and R (version 4.2.0) for single cell RNA seq analysis. All statistical tests are stated in the figure legends and/or related Methods sections. All statistical tests were two-tailed unless otherwise stated.

Data and Materials Availability

scRNA-seq data for epithelial cells from the Southampton dataset from 10 HNSCC cases and 7 matched healthy tonsil samples) are available here: https://zenodo.org/doi/10.5281/zenodo.13742281. Validation/external scRNA-seq data-sets are available for healthy lung and oesophagus (Madissoon *et al*, 2019) at Human Cell Atlas Data Coordination Platform and NCBI BIOPROJECT accession code PRJEB31843, and the following at the Gene Expression Omnibus (GEO): breast (GSE176078) (Wu *et al*, 2021);

910 healthy skin (GSE130973) (Solé-Boldo *et al*, 2020); bladder squamous cell carcinoma
911 (GSE190888) (Luo *et al*, 2022); head and neck squamous cell carcinoma (GSE16469082 and
912 GSE18222781); lung carcinoma (GSE131907, GSE136246, GSE148071, GSE153935,
913 GSE127465, GSE119911) (Prazanowska & Lim, 2023) collected at
914 https://doi.org/10.6084/m9.figshare.c.6222221.v3; oesophageal squamous cell carcinoma
915 (GSE160269) (Zhang *et al*, 2021) Cancer cell line data were obtained at
916 https://discover.nci.nih.gov/rsconnect/cellminercdb/ (accessed 31/07/2023). ChIP-seq data
917 were obtained from the Cistrome Data Browser (http://cistrome.org/db/#/). *APOBEC3A* KO
918 NIKS clones and the plasmids used to generate them are available from the authors upon
919 request.
920
921 **Acknowledgements**
922 This work was supported by funding to T.R.F from the UK Research and Innovation
923 Biotechnology and Biosciences Research Council (BB/V010271/2) and the Rosetrees Trust
924 (M229, PhD2020\100002, CF-2021-2\101), to G.J.T from Cancer Research UK (DRCNPG-
925 Jun22\100004) and to RSH from the National Cancer Institute (NCI P01-CA234228) and a
926 Recruitment of Established Investigators Award from the Cancer Prevention and Research
927 Institute of Texas (CPRIT RR220053). R.S.H is an Investigator of the Howard Hughes Medical
928 Institute and the Ewing Halsell President's Council Distinguished Chair at University of Texas
929 Health San Antonio. P.P. was supported by a CASE studentship from the BBSRC South Coast
930 Biosciences Doctoral Training Partnership (BB/T008768/1) and AstraZeneca. D.A., Academic
931 Clinical Fellow (ACF-2023-26-009) is funded by Health Education England (HEE) / NIHR for
932 this research project. The views expressed in this publication are those of the authors and
933 not necessarily those of the NIHR, NHS or the UK Department of Health and Social Care. We

would like to thank the Research Histology Group, Dept of Cellular Pathology, University Hospital Southampton, the Faculty of Medicine Tissue Bank, University of Southampton, and Bio-R Bioinformatics Research Facility, University of Southampton. The authors would also like to thank Holly McCarron for her assistance with the design and realisation of the graphical abstract.

Disclosure and Competing Interests

T.R.F. is an advisory board member of and holds stock options in APOBEC Discovery Ltd.

References

Aibar S, González-Blas CB, Moerman T, Huynh-Thu VA, Imrichova H, Hulselmans G, Rambow F, Marine JC, Geurts P, Aerts J, *et al* (2017) SCENIC: single-cell regulatory network inference and clustering. *Nature Methods* 14: 1083–1086

Alexandrov LB, Nik-Zainal S, Wedge DC, Aparicio SAJR, Behjati S, Biankin A V., Bignell GR, Bolli N, Borg A, Børresen-Dale A-L, *et al* (2013) Signatures of mutational processes in human cancer. *Nature* 500: 415–421

Allen-Hoffmann BL, Schlosser SJ, Ivarie CAR, Meisner LF, O'Connor SL & Sattler CA (2000) Normal Growth and Differentiation in a Spontaneously Immortalized Near-Diploid Human Keratinocyte Cell Line, NIKS. *Journal of Investigative Dermatology* 114: 444–455

Aynaud M-M, Suspène R, Vidalain P-O, Mussil B, Guétard D, Tangy F, Wain-Hobson S & Vartanian J-P (2012) Human Tribbles 3 protects nuclear DNA from cytidine deamination by APOBEC3A. *J Biol Chem* 287: 39182–92

Barretina J, Caponigro G, Stransky N, Venkatesan K, Margolin AA, Kim S, Wilson CJ, Lehár J, Kryukov G V., Sonkin D, *et al* (2012) The Cancer Cell Line Encyclopedia enables predictive modelling of anticancer drug sensitivity. *Nature* 483: 603–607

Bernstein BE, Stamatoyannopoulos JA, Costello JF, Ren B, Milosavljevic A, Meissner A, Kellis M, Marra MA, Beaudet AL, Ecker JR, *et al* (2010) The NIH Roadmap Epigenomics Mapping Consortium. *Nature Biotechnology* 28: 1045–1048

Boglev Y, Wilanowski T, Caddy J, Parekh V, Auden A, Darido C, Hislop NR, Cangkrama M, Ting SB & Jane SM (2011) The unique and cooperative roles of the Grainy head-like transcription factors in epidermal development reflect unexpected target gene specificity. *Dev Biol* 349: 512–522

Brown WL, Law EK, Argyris PP, Carpenter MA, Levin-Klein R, Ranum AN, Molan AM, Forster CL, Anderson BD, Lackey L, *et al* (2019) A Rabbit Monoclonal Antibody against the Antiviral and Cancer Genomic DNA Mutating Enzyme APOBEC3B. *Antibodies* 8: 47

969 Buisson R, Langenbucher A, Bowen D, Kwan EE, Benes CH, Zou L & Lawrence MS (2019)
970 Passenger hotspot mutations in cancer driven by APOBEC3A and mesoscale genomic
971 features. *Science* 364 eaaw2872
972 Burns MB, Lackey L, Carpenter MA, Rathore A, Land AM, Leonard B, Refsland EW,
973 Kotandeniya D, Tretyakova N, Nikas JB, *et al* (2013a) APOBEC3B is an enzymatic source
974 of mutation in breast cancer. *Nature* 494: 366–370
975 Burns MB, Temiz NA & Harris RS (2013b) Evidence for APOBEC3B mutagenesis in multiple
976 human cancers. *Nat Genet* 45: 977
977 Cable DM, Murray E, Zou LS, Goeva A, Macosko EZ, Chen F & Irizarry RA (2021) Robust
978 decomposition of cell type mixtures in spatial transcriptomics. *Nature Biotechnology*
979 40: 517–526
980 Caddy J, Wilanowski T, Darido C, Dworkin S, Ting SB, Zhao Q, Rank G, Auden A, Srivastava S,
981 Papenfuss TA, *et al* (2010) Epidermal Wound Repair Is Regulated by the Planar Cell
982 Polarity Signaling Pathway. *Dev Cell* 19: 138–147
983 Carpenter MA, Temiz NA, Ibrahim MA, Jarvis MC, Brown MR, Argyris PP, Brown WL, Starrett
984 GJ, Yee D & Harris RS (2023) Mutational impact of APOBEC3A and APOBEC3B in a
985 human cell line and comparisons to breast cancer. *PLoS Genet* 19: e1011043
986 Caswell DR, Gui P, Mayekar MK, Law EK, Pich O, Bailey C, Boumelha J, Kerr DL, Blakely CM,
987 Manabe T, *et al* (2023) The role of APOBEC3B in lung tumor evolution and targeted
988 cancer therapy resistance. *Nature Genetics* 56: 60–73
989 Cescon DW, Haibe-Kains B & Mak TW (2015) APOBEC3B expression in breast cancer reflects
990 cellular proliferation, while a deletion polymorphism is associated with immune
991 activation. *Proc Natl Acad Sci U S A* 112: 2841–2846
992 Chan K, Roberts SA, Klimczak LJ, Sterling JF, Saini N, Malc EP, Kim J, Kwiatkowski DJ, Fargo
993 DC, Mieczkowski PA, *et al* (2015) An APOBEC3A hypermutation signature is
994 distinguishable from the signature of background mutagenesis by APOBEC3B in human
995 cancers. *Nat Genet* 47: 1067–1072
996 Chen H, Lilley CE, Yu Q, Lee D V., Chou J, Narvaiza I, Landau NR & Weitzman MD (2006)
997 APOBEC3A is a potent inhibitor of adeno-associated virus and retrotransposons.
998 *Current Biology* 16: 480–485
999 Chen Y-T & Bradley A (2000) A New Positive/Negative Selectable Marker, *puΔtk*, for Use in
1000 Embryonic Stem Cells *Genesis* 28: 31-35.
1001 Cheng AZ, Yockteng-Melgar J, Jarvis MC, Malik-Soni N, Borozan I, Carpenter MA, McCann JL,
1002 Ebrahimi D, Shaban NM, Marcon E, *et al* (2018) Epstein–Barr virus BORF2 inhibits
1003 cellular APOBEC3B to preserve viral genome integrity. *Nature Microbiology* 4: 78–88
1004 Cong L, Ran FA, Cox D, Lin S, Barretto R, Habib N, Hsu PD, Wu X, Jiang W, Marraffini LA, *et al*
1005 (2013) Multiplex genome engineering using CRISPR/Cas systems. *Science* 339: 819–823
1006 Conticello SG (2008) The AID/APOBEC family of nucleic acid mutators. *Genome Biol* 9: 229
1007 Cortez LM, Brown AL, Dennis MA, Collins CD, Brown AJ, Mitchell D, Mertz TM & Roberts SA
1008 (2019) APOBEC3A is a prominent cytidine deaminase in breast cancer. *PLoS Genet* 15:
1009 e1008545
1010 Darido C, Georgy SR, Wilanowski T, Dworkin S, Auden A, Zhao Q, Rank G, Srivastava S, Finlay
1011 MJ, Papenfuss AT, *et al* (2011) Targeting of the Tumor Suppressor GRHL3 by a miR-21-
1012 Dependent Proto-Oncogenic Network Results in PTEN Loss and Tumorigenesis. *Cancer*
1013 *Cell* 20: 635–648

Deprez M, Zaragosi LE, Truchi M, Becavin C, García SR, Arguel MJ, Plaisant M, Magnone V, Lebrigand K, Abelanet S, *et al* (2020) A single-cell atlas of the human healthy airways. *Am J Respir Crit Care Med* 202: 1636–1645

Doorbar J, Quint W, Banks L, Bravo IG, Stoler M, Broker TR & Stanley MA (2012) The Biology and Life-Cycle of Human Papillomaviruses. *Vaccine* 30: F55–F70

Dunham I, Kundaje A, Aldred SF, Collins PJ, Davis CA, Doyle F, Epstein CB, Frietze S, Harrow J, Kaul R, *et al* (2012) An integrated encyclopedia of DNA elements in the human genome. *Nature* 489: 57–74

Durfee C, Temiz NA, Levin-Klein R, Argyris PP, Alsøe L, Carracedo S, Alonso de la Vega A, Proehl J, Holzhauer AM, Seeman ZJ, *et al* (2023) Human APOBEC3B promotes tumor development in vivo including signature mutations and metastases. *Cell Rep Med* 4: 101211

Edington KG, Loughran OP, Berry IJ & Parkinson EK (1995) Cellular immortality: A late event in the progression of human squamous cell carcinoma of the head and neck associated with p53 alteration and a high frequency of allele loss. *Mol Carcinog* 13: 254–265

Ernst J, Kheradpour P, Mikkelsen TS, Shoresh N, Ward LD, Epstein CB, Zhang X, Wang L, Issner R, Coyne M, *et al* (2011) Mapping and analysis of chromatin state dynamics in nine human cell types. *Nature* 473: 43–49

Faden DL, Thomas S, Cantalupo PG, Agrawal N, Myers J & DeRisi J (2017) Multi-modality analysis supports APOBEC as a major source of mutations in head and neck squamous cell carcinoma. *Oral Oncol* 74: 8–14

Franzén O, Gan LM & Björkegren JLM (2019) PanglaoDB: a web server for exploration of mouse and human single-cell RNA sequencing data. *Database* 2019: 46

Georgy SR, Cangkrama M, Srivastava S, Partridge D, Auden A, Dworkin S, McLean CA, Jane SM & Darido C (2015) Identification of a Novel Proto-oncogenic Network in Head and Neck Squamous Cell Carcinoma. *Journal of the National Cancer Institute* 107: djv152

Georgy SR, Rudiatmoko DR, Auden A, Partridge D, Butt T, Srivastava S, Wong N, Swaroop D, Carpinelli MR, Bogeski M, *et al* (2023) Identification of a Novel GRHL3/HOPX/Wnt/β-Catenin Proto-oncogenic Axis in Squamous Cell Carcinoma of the Esophagus. *Cell Mol Gastroenterol Hepatol* 15: 1051–1069

Ghandi M, Huang FW, Jané-Valbuena J, Kryukov G V., Lo CC, McDonald ER, Barretina J, Gelfand ET, Bielski CM, Li H, *et al* (2019) Next-generation characterization of the Cancer Cell Line Encyclopedia. *Nature* 569: 503–508

Gordon WM, Zeller MD, Klein RH, Swindell WR, Ho H, Espetia F, Gudjonsson JE, Baldi PF & Andersen B (2014) A GRHL3-regulated repair pathway suppresses immune-mediated epidermal hyperplasia. *J Clin Invest* 124: 5205–5218

Green AM, Budagyan K, Hayer KE, Reed MA, Savani MR, Wertheim GB & Weitzman MD (2017) Cytosine deaminase APOBEC3A sensitizes leukemia cells to inhibition of the DNA replication checkpoint. *Cancer Res* 77: 4579–4588

Green AM, Landry S, Budagyan K, Avgousti DC, Shalhout S, Bhagwat AS & Weitzman MD (2016) APOBEC3A damages the cellular genome during DNA replication. *Cell Cycle* 15: 998–1008

Green AM & Weitzman MD (2019) The spectrum of APOBEC3 activity: From anti-viral agents to anti-cancer opportunities. *DNA Repair (Amst)* 83: 102700

Hafemeister C & Satija R (2019) Normalization and variance stabilization of single-cell RNA-seq data using regularized negative binomial regression. *Genome Biol* 20: 1–15

Haradhvala NJ, Polak P, Stojanov P, Covington KR, Shinbrot E, Hess JM, Rheinbay E, Kim J, Maruvka YE, Braunstein LZ, *et al* (2016) Mutational Strand Asymmetries in Cancer Genomes Reveal Mechanisms of DNA Damage and Repair. *Cell* 164: 538–549

Harris RS & Dudley JP (2015) APOBECs and virus restriction. *Virology* 479–480: 131–145

Henderson S, Chakravarthy A, Su X, Boshoff C & Fenton TR (2014) APOBEC-Mediated Cytosine Deamination Links PIK3CA Helical Domain Mutations to Human Papillomavirus-Driven Tumor Development. *Cell Rep* 7: 1833–1841

Henderson S & Fenton T (2015) APOBEC3 genes: Retroviral restriction factors to cancer drivers. *Trends Mol Med* 21: 274–284

Hirabayashi S, Shirakawa K, Horisawa Y, Matsumoto T, Matsui H, Yamazaki H, Sarca AD, Kazuma Y, Nomura R, Konishi Y, *et al* (2021) APOBEC3B is preferentially expressed at the G2/M phase of cell cycle. *Biochem Biophys Res Commun* 546: 178–184

Hislop NR, Caddy J, Ting SB, Auden A, Vasudevan S, King SL, Lindeman GJ, Visvader JE, Cunningham JM & Jane SM (2008) Grhl3 and Lmo4 play coordinate roles in epidermal migration. *Dev Biol* 321: 263–272

Hoopes JI, Cortez LM, Mertz TM, Malc EP, Mieczkowski PA & Roberts SA (2016) APOBEC3A and APOBEC3B Preferentially Deaminate the Lagging Strand Template during DNA Replication. *Cell Rep* 14: 1273–1282

Hopkin AS, Gordon W, Klein RH, Espitia F, Daily K, Zeller M, Baldi P & Andersen B (2012) GRHL3/GET1 and Trithorax Group Members Collaborate to Activate the Epidermal Progenitor Differentiation Program. *PLoS Genet* 8: e1002829

Isozaki H, Sakhtemani R, Abbasi A, Nikpour N, Stanzione M, Oh S, Langenbucher A, Monroe S, Su W, Cabanos HF, *et al* (2023) Therapy-induced APOBEC3A drives evolution of persistent cancer cells. *Nature* 620: 393–401

Jalili P, Bowen D, Langenbucher A, Park S, Aguirre K, Corcoran RB, Fleischman AG, Lawrence MS, Zou L & Buisson R (2020) Quantification of ongoing APOBEC3A activity in tumor cells by monitoring RNA editing at hotspots. *Nat Commun* 11: 2971

Jarmuz A, Chester A, Bayliss J, Gisbourne J, Dunham I, Scott J & Navaratnam N (2002) An Anthropoid-Specific Locus of Orphan C to U RNA-Editing Enzymes on Chromosome 22. *Genomics* 79: 285–296

Kabir MF, Karami AL, Cruz-Acuña R, Klochkova A, Saxena R, Mu A, Murray MG, Cruz J, Fuller AD, Clevenger MH, *et al* (2022) Single cell transcriptomic analysis reveals cellular diversity of murine esophageal epithelium. *Nature Communications* 13: 1–15

Kang SYC, Kannan N, Zhang L, Martinez V, Rosin MP & Eaves CJ (2015) Characterization of Epithelial Progenitors in Normal Human Palatine Tonsils and Their HPV16 E6/E7-Induced Perturbation. *Stem Cell Reports* 5: 1210–1225

Klein RH, Lin Z, Hopkin AS, Gordon W, Tsoi LC, Liang Y, Gudjonsson JE & Andersen B (2017) GRHL3 binding and enhancers rearrange as epidermal keratinocytes transition between functional states. *PLoS Genet* 13: e1006745

Koning FA, Newman ENC, Kim E-Y, Kunstman KJ, Wolinsky SM & Malim MH (2009) Defining APOBEC3 Expression Patterns in Human Tissues and Hematopoietic Cell Subsets. *J Virol* 83: 9474–9485

Kono T, Hoover P, Poropatich K, Paunesku T, Mittal BB, Samant S & Laimins LA (2020) Activation of DNA damage repair factors in HPV positive oropharyngeal cancers. *Virology* 547: 27–34

Kouwenhoven EN, Oti M, Niehues H, van Heeringen SJ, Schalkwijk J, Stunnenberg HG, van Bokhoven H & Zhou H (2015) Transcription factor p63 bookmarks and regulates dynamic enhancers during epidermal differentiation. *EMBO Rep* 16: 863–878

Kudryavtseva EI, Sugihara TM, Wang N, Lasso RJ, Gudnason JF, Lipkin SM & Andersen B (2003) Identification and characterization of Grainyhead-like epithelial transactivator (GET-1), a novel mammalian Grainyhead-like factor. *Developmental Dynamics* 226: 604–617

Kumar N, Mishra B, Athar M & Mukhtar S (2021) Inference of Gene Regulatory Network from Single-Cell Transcriptomic Data Using pySCENIC. *Methods in Molecular Biology* 2328: 171–182

Kürten CHL, Kulkarni A, Cillo AR, Santos PM, Roble AK, Onkar S, Reeder C, Lang S, Chen X, Duvvuri U, *et al* (2021) Investigating immune and non-immune cell interactions in head and neck tumors by single-cell RNA sequencing. *Nature Communications* 12: 1–16

Law EK, Levin-Klein R, Jarvis MC, Kim H, Argyris PP, Carpenter MA, Starrett GJ, Temiz NA, Larson LK, Durfee C, *et al* (2020) APOBEC3A catalyzes mutation and drives carcinogenesis in vivo. *Journal of Experimental Medicine* 217: e20200261

Lejeune N, Mathieu S, Decloux A, Poulain F, Blockx Z, Raymond KA, Willemart K, Vartanian JP, Suspène R & Gillet NA (2023) The APOBEC3B cytidine deaminase is an adenovirus restriction factor. *PLoS Pathog* 19: e1011156

Lin L, Holmes B, Shen MW, Kammeron D, Geijsen N, Gifford DK & Sherwood RI (2020) Comprehensive Mapping of Key Regulatory Networks that Drive Oncogene Expression. *Cell Rep* 33: 108426

Lin M, Sade-Feldman M, Wirth L, Lawrence MS & Faden DL (2022) Single-cell transcriptomic profiling for inferring tumor origin and mechanisms of therapeutic resistance. *NPJ Precis Oncol* 6: 1–7

Lucifora J, Xia Y, Reisinger F, Zhang K, Stadler D, Cheng X, Sprinzl MF, Koppensteiner H, Makowska Z & Volz T (2014) Specific and nonhepatotoxic degradation of nuclear hepatitis B virus cccDNA. *Science* 343: 1221–1228

Luna A, Elloumi F, Varma S, Wang Y, Rajapakse VN, Aladjem MI, Robert J, Sander C, Pommier Y & Reinhold WC (2021) CellMiner Cross-Database (CellMinerCDB) version 1.2: Exploration of patient-derived cancer cell line pharmacogenomics. *Nucleic Acids Res* 49: D1083–D1093

Luo Y, Tao T, Tao R, Huang G & Wu S (2022) Single-Cell Transcriptome Comparison of Bladder Cancer Reveals Its Ecosystem. *Front Oncol* 12: 818147

MacCarthy-Morrogh L & Martin P (2020) The hallmarks of cancer are also the hallmarks of wound healing. *Sci Signal* 13: 8690

Madissoon E, Wilbrey-Clark A, Miragaia RJ, Saeb-Parsy K, Mahbubani KT, Georgakopoulos N, Harding P, Polanski K, Huang N, Nowicki-Osuch K, *et al* (2019) ScRNA-seq assessment of the human lung, spleen, and esophagus tissue stability after cold preservation. *Genome Biol* 21: 1–16

Madsen P, Celis JE, Rasmussen HH, Vorum H, Anant S, Gromov P, Dumanski JP, Tommerup N, Collins JE, Wright CL, *et al* (1999) Psoriasis Upregulated Phorbolin-1 Shares Structural but not Functional Similarity to the mRNA-Editing Protein Apobec-1. *Journal of Investigative Dermatology* 113: 162–169

Mertz TM, Collins CD, Dennis M, Coxon M & Roberts SA (2022) APOBEC-Induced Mutagenesis in Cancer. *Annu Rev Genet* 56: 229–252

Morganella S, Alexandrov LB, Glodzik D, Zou X, Davies H, Staaf J, Sieuwerts AM, Brinkman AB, Martin S, Ramakrishna M, *et al* (2016) The topography of mutational processes in breast cancer genomes. *Nat Commun* 7: 11383

Mori S, Takeuchi T, Ishii Y, Yugawa T, Kiyono T, Nishina H & Kukimoto I (2017) Human Papillomavirus 16 E6 Upregulates APOBEC3B via the TEAD Transcription Factor. *J Virol* 91: e02413-16

Naumann JA, Argyris PP, Carpenter MA, Gupta HB, Chen Y, Temiz NA, Zhou Y, Durfee C, Proehl J, Koniar BL, *et al* (2023) DNA Deamination Is Required for Human APOBEC3A-Driven Hepatocellular Carcinoma In Vivo. *Int J Mol Sci* 24: 9305

Novakovic B, Habibi E, Wang SY, Arts RJW, Davar R, Megchelenbrink W, Kim B, Kuznetsova T, Kox M, Zwaag J, *et al* (2016) β-Glucan Reverses the Epigenetic State of LPS-Induced Immunological Tolerance. *Cell* 167: 1354-1368.e14

Nurminen V, Neme A, Seuter S & Carlberg C (2018) The impact of the vitamin D-modulated epigenome on VDR target gene regulation. *Biochimica et Biophysica Acta (BBA) - Gene Regulatory Mechanisms* 1861: 697–705

Oh S, Bournique E, Bowen D, Jalili P, Sanchez A, Ward I, Dananberg A, Manjunath L, Tran GP, Semler BL, *et al* (2021) Genotoxic stress and viral infection induce transient expression of APOBEC3A and pro-inflammatory genes through two distinct pathways. *Nature Communications* 12: 1–17

Oh S & Buisson R (2022) A digital PCR-based protocol to detect and quantify RNA editing events at hotspots. *STAR Protoc* 3: 101148

Patel AP, Tirosh I, Trombetta JJ, Shalek AK, Gillespie SM, Wakimoto H, Cahill DP, Nahed B V., Curry WT, Martuza RL, *et al* (2014) Single-cell RNA-seq highlights intratumoral heterogeneity in primary glioblastoma. *Science* 344: 1396–1401

Peng G, Greenwell-Wild T, Nares S, Jin W, Ke JL, Rangel ZG, Munson PJ & Wahl SM (2007) Myeloid differentiation and susceptibility to HIV-1 are linked to APOBEC3 expression. *Blood* 110: 393–400

Periyasamy M, Patel H, Lai C-F, Nguyen VTM, Nevedomskaya E, Harrod A, Russell R, Remenyi J, Ochocka AM, Thomas RS, *et al* (2015) APOBEC3B-Mediated Cytidine Deamination Is Required for Estrogen Receptor Action in Breast Cancer. *Cell Rep* 13: 108–121

Periyasamy M, Singh AK, Gemma C, Farzan R, Allsopp RC, Shaw JA, Charmsaz S, Young LS, Cunnea P, Coombes RC, *et al* (2020) Induction of APOBEC3B expression by chemotherapy drugs is mediated by DNA-PK-directed activation of NF-κB. *Oncogene* 40: 1077–1090

Periyasamy M, Singh AK, Gemma C, Kranjec C, Farzan R, Leach DA, Navaratnam N, Pálinkás HL, Vertessy BG, Fenton TR, *et al* (2017) P53 controls expression of the DNA deaminase APOBEC3B to limit its potential mutagenic activity in cancer cells. *Nucleic Acids Res* 45: 11056-11069

Petljak M, Alexandrov LB, Brammeld JS, Price S, Wedge DC, Grossmann S, Dawson KJ, Ju YS, Iorio F, Tubio JMC, *et al* (2019) Characterizing Mutational Signatures in Human Cancer Cell Lines Reveals Episodic APOBEC Mutagenesis. *Cell* 176: 1282-1294.e20

Petljak M, Dananberg A, Chu K, Bergstrom EN, Striepen J, von Morgen P, Chen Y, Shah H, Sale JE, Alexandrov LB, *et al* (2022a) Mechanisms of APOBEC3 mutagenesis in human cancer cells. *Nature* 607: 799–807

Petljak M, Green AM, Maciejowski J & Weitzman MD (2022b) Addressing the benefits of inhibiting APOBEC3-dependent mutagenesis in cancer. *Nat Genet* 54: 1599–1608

Petljak M & Maciejowski J (2020) Molecular origins of APOBEC-associated mutations in cancer. *DNA Repair (Amst)* 94: 102905

Peus D, Hamacher L & Pittelkow MR (1997) EGF-receptor tyrosine kinase inhibition induces keratinocyte growth arrest and terminal differentiation. *J Invest Dermatol* 109: 751–756

Poumay Y & Pittelkow MR (1995) Cell Density and Culture Factors Regulate Keratinocyte Commitment to Differentiation and Expression of Suprabasal K1/K10 Keratins. *Journal of Investigative Dermatology* 104: 271–276

Prazanowska KH & Lim S Bin (2023) An integrated single-cell transcriptomic dataset for non-small cell lung cancer. *Scientific Data* 10: 1–15

Puram S V., Mints M, Pal A, Qi Z, Reeb A, Gelev K, Barrett TF, Gerndt S, Liu P, Parikh AS, *et al* (2023) Cellular states are coupled to genomic and viral heterogeneity in HPV-related oropharyngeal carcinoma. *Nature Genetics* 55: 640–650

Rasmussen HH & Celis JE (1993) Evidence for an Altered Protein Kinase C (PKC) Signaling Pathways in Psoriasis. *Journal of Investigative Dermatology* 101: 560–566

Refsland EW, Stenglein MD, Shindo K, Albin JS, Brown WL & Harris RS (2010) Quantitative profiling of the full APOBEC3 mRNA repertoire in lymphocytes and tissues: implications for HIV-1 restriction. *Nucleic Acids Res* 38: 4274–4284

Roberts SA, Lawrence MS, Klimczak LJ, Grimm SA, Fargo D, Stojanov P, Kiezun A, Kryukov G V, Carter SL & Saksena G (2013) An APOBEC cytidine deaminase mutagenesis pattern is widespread in human cancers. *Nat Genet* 45: 970

Rochman M, Wen T, Kotliar M, Dexheimer PJ, Morgenstern NBB, Caldwell JM, Lim HW & Rothenberg ME (2022) Single-cell RNA-Seq of human esophageal epithelium in homeostasis and allergic inflammation. *JCI Insight* 7 e159093

Roelofs PA, Goh CY, Chua BH, Jarvis MC, Stewart TA, McCann JL, McDougle RM, Carpenter MA, Martens JWM, Span PN, *et al* (2020) Characterization of the mechanism by which the RB/E2F pathway controls expression of the cancer genomic dna deaminase APOBEC3B. *Elife* 9: 1–64

Roelofs PA, Timmermans MAM, Stefanovska B, den Boestert MA, van den Borne AWM, Balcioglu HE, Trapman AM, Harris RS, Martens JWM & Span PN (2023) Aberrant APOBEC3B Expression in Breast Cancer Is Linked to Proliferation and Cell Cycle Phase. *Cells* 12: 1185

Rubin AJ, Barajas BC, Furlan-Magaril M, Lopez-Pajares V, Mumbach MR, Howard I, Kim DS, Boxer LD, Cairns J, Spivakov M, *et al* (2017) Lineage-specific dynamic and pre-established enhancer–promoter contacts cooperate in terminal differentiation. *Nature Genetics* 49: 1522–1528

Schnepp BC, Jensen RL, Chen C-L, Johnson PR & Clark KR (2005) Characterization of Adeno-Associated Virus Genomes Isolated from Human Tissues. *J Virol* 79: 14793–14803

Scholz GM, Sulaiman NS, Al Baiiaty S, Kwa MQ & Reynolds EC (2016) A novel regulatory relationship between RIPK4 and ELF3 in keratinocytes. *Cell Signal* 28: 1916–1922

Seplyarskiy VB, Soldatov RA, Popadin KY, Antonarakis SE, Bazykin GA & Nikolaev SI (2016) APOBEC-induced mutations in human cancers are strongly enriched on the lagging DNA strand during replication. *Genome Res* 26: 174–82

Shi C, Ray-Jones H, Ding J, Duffus K, Fu Y, Gaddi VP, Gough O, Hankinson J, Martin P, McGovern A, *et al* (2021) Chromatin Looping Links Target Genes with Genetic Risk Loci for Dermatological Traits. *Journal of Investigative Dermatology* 141: 1975–1984

Siriwardena SU, Perera MLW, Senevirathne V, Stewart J & Bhagwat AS (2018) A tumor promoting phorbol ester causes a large increase in APOBEC3A and a moderate increase in APOBEC3B expression in a normal human keratinocyte cell line without increasing genomic uracils. *Mol Cell Biol* 39: e00238-18

Smith NJ & Fenton TR (2019) The APOBEC3 genes and their role in cancer: Insights from human papillomavirus. *J Mol Endocrinol* 62: R269–R287

Solé-Boldo L, Raddatz G, Schütz S, Mallm JP, Rippe K, Lonsdorf AS, Rodríguez-Paredes M & Lyko F (2020) Single-cell transcriptomes of the human skin reveal age-related loss of fibroblast priming. *Communications Biology* 3: 1–12

Stanley MA, Browne HM, Appleby M & Minson AC (1989) Properties of a non-tumorigenic human cervical keratinocyte cell line. *Int J Cancer* 43: 672–676

Stewart JA, Schauer G & Bhagwat AS (2020) Visualization of uracils created by APOBEC3A using UdgX shows colocalization with RPA at stalled replication forks. *Nucleic Acids Res* 48: e118–e118

Suspène R, Aynaud MM, Guétard D, Henry M, Eckhoff G, Marchio A, Pineau P, Dejean A, Vartanian JP & Wain-Hobson S (2011) Somatic hypermutation of human mitochondrial and nuclear DNA by APOBEC3 cytidine deaminases, a pathway for DNA catabolism. *Proc Natl Acad Sci U S A* 108: 4858–4863

Swanton C, McGranahan N, Starrett GJ & Harris RS (2015) APOBEC Enzymes: Mutagenic Fuel for Cancer Evolution and Heterogeneity. *Cancer Discov* 5: 704–712

Taura M, Frank JA, Takahashi T, Kong Y, Kudo E, Song E, Tokuyama M & Iwasaki A (2022) APOBEC3A regulates transcription from interferon-stimulated response elements. *Proc Natl Acad Sci U S A* 119: e2011665119

Taylor BJ, Nik-Zainal S, Wu YL, Stebbings LA, Raine K, Campbell PJ, Rada C, Stratton MR & Neuberger MS (2013) DNA deaminases induce break-associated mutation showers with implication of APOBEC3B and 3A in breast cancer kataegis. *Elife* 2: e00534

The Cancer Genome Atlas Network (2015) Comprehensive genomic characterization of head and neck squamous cell carcinomas. *Nature* 517: 576–582

Ting S, Caddy J, Hislop N, Wilanowski T & Auden A (2005) A homolog of Drosophila grainy head is essential for epidermal integrity in mice. *Science* 308, 411-413

Vartanian J-P, Guétard D, Henry M & Wain-Hobson S (2008) Evidence for editing of human papillomavirus DNA by APOBEC3 in benign and precancerous lesions. *Science* 320: 230–233

Vieira VC, Leonard B, White EA, Starrett GJ, Temiz NA, Lorenz LD, Lee D, Soares MA, Lambert PF, Howley PM, *et al* (2014) Human papillomavirus E6 triggers upregulation of the antiviral and cancer genomic DNA deaminase APOBEC3B. *mBio* 5: e02234-14

Wakae K, Nishiyama T, Kondo S, Izuka T, Que L, Chen C, Kase K, Kitamura K, Mohiuddin M, Wang Z, *et al* (2018) Keratinocyte differentiation induces APOBEC3A, 3B, and mitochondrial DNA hypermutation. *Sci Rep* 8: 9745

Wang Z, Wakae K, Kitamura K, Aoyama S, Liu G, Koura M, Monjurul AM, Kukimoto I & Muramatsu M (2014) APOBEC3 deaminases induce hypermutation in human papillomavirus 16 DNA upon beta interferon stimulation. *J Virol* 88: 1308–1317

Warren CJ, Xu T, Guo K, Griffin LM, Westrich JA, Lee D, Lambert PF, Santiago ML & Pyeon D (2015) APOBEC3A functions as a restriction factor of human papillomavirus. *J Virol* 89: 688–702

Wu SZ, Al-Eryani G, Roden DL, Junankar S, Harvey K, Andersson A, Thennavan A, Wang C, Torpy JR, Bartonicek N, *et al* (2021) A single-cell and spatially resolved atlas of human breast cancers. *Nature Genetics* 53: 1334–1347

Yu Z, Bhandari A, Mannik J, Pham T, Xu X & Andersen B (2008) Grainyhead-like factor Get1/Grhl3 regulates formation of the epidermal leading edge during eyelid closure. *Dev Biol* 319: 56–67

Yu Z, Lin K, Bhandari A, Spencer J & Xu X (2006) The Grainyhead-like epithelial transactivator Get-1/Grhl3 regulates epidermal terminal differentiation and interacts functionally with LMO4. *Dev Biol* 299: 122-136

Zhang X, Peng L, Luo Y, Zhang S, Pu Y, Chen Y, Guo W, Yao J, Shao M, Fan W, *et al* (2021) Dissecting esophageal squamous-cell carcinoma ecosystem by single-cell transcriptomic analysis. *Nature Communications* 12: 1–17

Figure Legends

Figure 1: *APOBEC3A* and *APOBEC3B* expression in scRNA-seq datasets representing normal and tumour epithelial cells from tissues in which cancers that display prominent APOBEC mutational signatures arise. The number above each pie chart represents the total number of epithelial cells in each dataset. The references for each dataset are provided in Table EV2.

Figure 2: *APOBEC3A* and *APOBEC3B* are expressed in different subsets of tonsillar epithelial cells

A) UMAP projection of 22,595 epithelial cells from oropharyngeal squamous cell carcinoma samples (n = 10; 18,619 malignant cells (red), 695 non-malignant cells (purple)), and matched normal tonsil (n = 7; 3,281 cells (blue)).

B) GOBP terms enriched amongst the sets of 100 genes that were co-expressed with either *APOBEC3A* or *APOBEC3B* in the 2,649 (after QC) epithelial cells from normal tonsil. Terms ranked by P value calculated by EnrichR package (Fisher Exact test bias corrected using the z-score of the deviation from the expected rank).

C) UMAP projection depicting four phenotypes (basal, proliferating, differentiating, terminally differentiated) displayed by the normal tonsillar epithelial cells in our dataset.

D) Marker genes used to identify the four epithelial phenotypes represented in panel C.

E) Violin plots of gene expression in individual tonsillar epithelial cells, and UMAP projections of the density of gene expression in the tonsillar epithelial subtypes. (**** = P < 0.0001, Wilcoxon's Rank Sum Test; Basal, n = 1,047; Proliferating, n = 353; Differentiating, n = 1,091; Terminally Differentiated, n = 158).

Figure 3: Keratinocyte cell cycle exit and initiation of differentiation is marked by a switch from *APOBEC3B* to *APOBEC3A* expression.

A) qRT-PCR-based gene expression measurements (n = 3) for *APOBEC3A* (P = 0.0002), *KRT10* (P = 0.0002), *IVL* (P < 0.0001), *APOBEC3B* (P = 0.0001), *MKI67* (P < 0.0001) and *MCM7* (P = 0.0033) in proliferating NIKS (Async) or following 48 hours of growth factor deprivation (Starved).

B) representative cell cycle profiles of Async and starved NIKS measured by PI staining and flow cytometry.

C) qRT-PCR-based gene expression measurements (n = 3) for *APOBEC3A* (P = 0.0036), *KRT10* (P = 0.0004), *IVL* (P = 0.0007), *APOBEC3B* (P = 0.9445), *MKI67* (P = 0.0032) and *MCM7* (P = 0.0001) following 24 hours of vehicle control (DMSO) or 100 nM afatinib treatment (EGFRi).

D) representative cell cycle profiles of DMSO and afatinib-treated NIKS measured by PI staining and flow cytometry.

E) qRT-PCR-based gene expression measurements (n = 3) for *APOBEC3A* (adjusted P values versus day 3 measurement: day 5 = 0.9960; day 7 = 0.0009; day 9 < 0.0001), *KRT10* (adjusted P values versus day 3 measurement: day 5 = 0.9518; day 7 = 0.0005; day 9 <

0.0001), *IVL* (adjusted P values versus day 3 measurement: day 5 = 0.9983; day 7 = 0.0035; day 9 < 0.0001), *APOBEC3B* (adjusted P values versus day 3 measurement: day 5 < 0.0001; day 7 < 0.0001; day 9 < 0.0001), *MKI67* (adjusted P values versus day 3 measurement: day 5 = 0.0001; day 7 < 0.0001; day 9 < 0.0001) and *MCM7* (adjusted P values versus day 3 measurement: day 5 < 0.0001; day 7 < 0.0001; day 9 < 0.0001) in NIKS collected 3, 5, 7, or 9 days after plating.

F) representative cell cycle profiles of NIKS collected 3, 5, 7, or 9 days after plating measured by PI staining and flow cytometry.

G) qRT-PCR measurements of *APOBEC3A* expression in primary human epidermal keratinocytes (NHEK) growing in FC medium and treated for 24 hr with vehicle control (DMSO) or 100 nM afatinib (EGFRi, P < 0.0001) or following growth factor deprivation for 48 hr (Starved, P = 0.0003).

H) Percentage of DDOST transcripts that were C>U edited at c558 in asynchronous growing NIKS (Async) and following 48 hours of growth factor withdrawal (starved) measured by digital PCR assay (n = 3; P < 0.0001). Error bars = SEM. * = P < 0.05; ** = P < 0.01; *** = P < 0.001; **** = P < 0.0001. Pairwise comparisons were performed using unpaired two-tailed t-tests in (A), (C) and (H). Comparisons of mRNA levels on days 5, 7 and 9 to day 3 in (E), and of mRNA levels in starved and afatinib-treated cells to DMSO-treated cells in (G) were performed using one-way ANOVA with Dunnett's multiple comparisons test.

Figure 4: Grainyhead-like transcription factor 3 is required for *APOBEC3A* expression during keratinocyte differentiation.

A) Heatmap showing those transcription factors (of the 363 with a SCENIC activity score in our scRNA-seq dataset from healthy tonsil epithelium) that were differentially active (fold

change > 1.1, adjusted P < 0.05, Wilcoxon Rank Sum test) between the clusters defined in Figure 2C (Bas. = basal; Pro. = proliferating; Diff. = differentiating; T.Diff. = terminally differentiated).

B) UMAPs showing GRHL3 transcription factor activity score from SCENIC (top) and *APOBEC3A* expression (bottom) in the Southampton scRNA-seq dataset from healthy tonsil epithelium. **C)** boxplot showing *APOBEC3A* expression stratified by SCENIC binary predictions of GRHL3 'off' or GRHL3 'on' (top; (**** = P < 0.0001, Wilcoxon's Rank Sum Test)) and histogram showing the number of cells in each of four groups: GRHL3 'off', no detectable *APOBEC3A* (A3A-/GRHL3-), n = 1,160; GRHL3 'on', no detectable *APOBEC3A* (A3A-/GRHL3+), n = 480; GRHL3 'off', *APOBEC3A* expressed (A3A+/GRHL-), n = 73, and GRHL3 'on', *APOBEC3A* expressed (A3A+/GRHL3+), n = 936 (bottom). Top, middle and bottom line of the boxplot represent the upper quartile (Q3), median, and lower quartile (Q1) respectively. The maximum value represented by the top whisker represents the highest observed data point within Q3 + (1.5 x (Q3-Q1)), and the minimum value represented by the bottom whisker represents the lowest situated point within Q1 - (1.5 x (Q3-Q1)). The dashed red line represents the mean.

D) qRT-PCR-based expression measurements (n = 3) of *APOBEC3A*, *GRHL3, IVL* and *ELF3* in NIKS transfected with control (NC#1) or *GRHL3*-specific siRNAs as indicated. Adjusted P values for comparisons between NC#1 and *GRHL3* siRNA #1: *APOBEC3A* = 0.0004; *GRHL3* < 0.0001; *IVL* < 0.0001; *ELF3* = 0.0072. Adjusted P values for comparisons between NC#1 and *GRHL3* siRNA #2: *APOBEC3A* = 0.0012; *GRHL3* < 0.0001; *IVL* < 0.0001; *ELF3* = 0.0052. Cells were treated with 100 nM afatinib for 24 hours prior to harvesting to induce differentiation.

(E) Percentage of DDOST transcripts that were C>U edited at c558 in in NIKS transfected with control (NC#1) or *GRHL3*-specific siRNAs as indicated (n = 3). Adjusted P values: NC#1 vs *GRHL3* siRNA #1 = 0.0072; NC#1 vs *GRHL3* siRNA #2 = 0.0099.

Gene expression (D) and DDOST editing (E) in *GRHL3* siRNA-transfected cells were compared with control siRNA-transfected cells using one-way ANOVA with Tukey's multiple comparisons test (error bars represent SEM; ** = P < 0.01, ***= P < 0.001 and **** = P < 0.0001).

F) ChIP-seq data for GHRL3, WDR5, H3K27Ac, H3K4Me1 and H3K4Me3 from keratinocytes and or monocytes and GeneHancer predicted regulatory regions (grey = enhancer, red = promoter) as indicated, spanning the *APOBEC3A* gene and a 33kb region upstream of the TSS (see main text for references to the datasets).

G) Stacked barplot showing the proportion of each cell type in the single cell atlas of healthy human airways from Deprez et al that express each selected gene.

Figure 5: GRHL3 regulates *APOBEC3A* expression in squamous cell carcinoma.

A) UMAPs heatmap showing gene expression of *APOBEC3A* and *IVL* and predicted activity of GRHL3 in scRNA-seq data from four independent tumour cohorts (3 HNSCC and one ESCC).

B) qRT-PCR-based gene expression measurements of *APOBEC3A* and *GRHL3* in sub-confluent BICR6 (top row) and BICR22 (bottom row) HNSCC cells transfected with control (NC#1) or *GRHL3*-specific siRNAs as indicated. Adjusted P values: NC#1 vs *GRHL3* siRNA #1 (*APOBEC3A*: BICR6 < 0.0001; BICR22 = 0.0145; *GRHL3*: BICR6 < 0.0001; BICR22 < 0.0001); NC#1 vs *GRHL3* siRNA #2 (*APOBEC3A*: BICR6 < 0.0001; BICR22 = 0.0035; *GRHL3*: BICR6 < 0.0001; BICR22 < 0.0001). Gene expression in *GRHL3* siRNA-transfected cells was compared with control siRNA-transfected cells using one-way ANOVA with Tukey's multiple

comparisons test (n = 3; error bars represent SEM; **** = P < 0.0001; ** = P < 0.01 and * = P < 0.05).

C) matrix showing the relationship between expression of the indicated genes in spatial transcriptomics data from the Southampton HNSCC cohort obtained using the Visium platform (10X Genomics).

D) Images displaying expression levels (Visium spot intensities) of selected genes in HN485, an HPV+ve HNSCC case from the Southampton cohort.

E) Immunohistochemistry with an antibody specific for APOBEC3A (left) and with an antibody that cross-reacts with APOBEC3A, APOBEC3B and APOBEC3G (right) in sections from the same tissue block from HN485 used for the Visium profiling displayed in part D.

F) Boxplot showing expression of *APOBEC3A* in those cells predicted to be in S-phase in normal tonsil and HNSCC, stratified by binary GRHL3 activity score (on/off). Cells shown in black are outliers relative to the distribution of expression in the cells from healthy tonsil. Inset: UMAP showing the predicted cell cycle phase for each cell in the Southampton HNSCC scRNA-seq dataset. Top, middle and bottom line of the boxplot represent the upper quartile (Q3), median, and lower quartile (Q1) respectively. The maximum value represented by the top whisker represents the highest observed data point within Q3 + (1.5 x (Q3-Q1)), and the minimum value represented by the bottom whisker represents the lowest situated point within Q1 - (1.5 x (Q3-Q1)). Healthy GRHL3 'OFF', n = 19; Healthy GRHL3 'ON', n = 173; Tumour GRHL3 'OFF', n = 98; Tumour GRHL3 'ON', n = 620.

Table 1: Primers used for qPCR, digital PCR, genotyping and/or plasmid construction.

Gene	Sequence
APOBEC3A (Forward)	5'-GAGAAGGGACAAGCACATGG-3'
APOBEC3A	5'-TGGATCCATCAAGTGTCTGG-3'

(Reverse)	
APOBEC3B (Forward)	5’-GACCCTTTGGTCCTTCGAC-3’
APOBEC3B (Reverse)	5’-GCACAGCCCCAGGAGAAG-3’
KRT10 (Forward)	5’-CCTGCTTCAGATCGACAATGCC-3'
KRT10 (Reverse)	5’-ATCTCCAGGTCAGCCTTGGTCA-3'
IVL (Forward)	5’-GGTCCAAGACATTCAACCAGCC-3'
IVL (Reverse)	5’-TCTGGACACTGCGGGTGGTTAT-3'
MKI67 (Forward)	5’-GAAAGAGTGGCAACCTGCCTTC-3'
MKI67 (Reverse)	5’-GCACCAAGTTTTACTACATCTGCC-3'
MCM7 (Forward)	5’-GCCAAGTCTCAGCTCCTGTCAT-3'
MCM7 (Reverse)	5’-CCTCTAAGGTCAGTTCTCCACTC-3'
ELF3 (Forward)	5’-CATGACCTACGAGAAGCTGAGC-3'
ELF3 (Reverse)	5’-GACTCTGGAGAACCTCTTCCTC-3'
GRHL3 (Forward)	5’-ACTGTGGAGCACATTGAGGAGG-3’
GRHL3 (Reverse)	5’-CTGTGCTCAGACAGTTTACGCC-3’
TBP (Forward)	5’-TTGAGGAAGTTGCTGAGAAGAG-3’
TBP (Reverse)	5’-CAGATAGCAGCACGGTATGAG-3’
TBP standard (Forward)	5'-CACTCACAGACTCTCACAACTG-3'
TBP standard (Reverse)	5'-GTCGTCTTCCTGAATCCCTTTAG-3'
DDOST (Forward)	5’- ACTGAGAACCTGCTGAAG-3’
DDOST (Reverse)	5’- AAGAGGATGGGATTTAGAGA-3’
DDOSTC558 Probe	5’-(HEX)-CAACCATCGTTGGGAAATC-(Q)-3′
DDOSTT558 Probe	5’-(FAM)-CCAACCATTGTTGGGAAATC-(Q)-3′
A3A N-term left sgRNA (sense)	5’- CACCGCTTGCGACTTGCTCAAGGCG-3’
A3A N-term left sgRNA (antisense)	5’-AAACCGCCTTGAGCAAGTCGCAAGC-3’
A3A N-term right sgRNA (sense)	5’-CACCGCACAGACCAGGAACCGAGAA-3’
A3A N-term right sgRNA (antisense)	5’-AAACTTCTCGGTTCCTGGTCTGTGC-3’
A3A deletion genotyping primer (Forward)	5’-TGAGCTCACACCAGAACCAC-3’
A3A deletion genotyping primer (Reverse)	5’-TAGAGCCCAGAGAAGGTCCC-3’

Expanded View Figure Legends

Figure EV1. *APOBEC3B* is predominantly co-expressed with proliferation markers *MKI67* and *MCM7* in cycling basal and suprabasal cells of the healthy human airway. Stacked barplot showing the proportion of each cell type in the single cell atlas of healthy human airways from Deprez et al that express each selected gene.

Figure EV2. *APOBEC3A* and *GRHL3* expression by cancer type in TCGA bulk RNA-seq data.

A) Boxplot ranked from highest median (left) to lowest median (right) for *APOBEC3A* gene expression.

B) Boxplot ranked from highest median (left) to lowest median (right) for *GRHL3* gene expression.

C) Boxplot ranked from highest median (left) to lowest median (right) for GRHL3 signature score based on the mean expression of 127 GRHL3 target genes identified in scRNA-seq SCENIC analysis. Each dot represents an individual tumour sample.

D) Spearman correlation coefficients for *APOBEC3A* and *GRHL3* expression in TCGA RNA-seq data.

E) Spearman correlation coefficients for *APOBEC3A* expression and GRHL3 signature score in TCGA RNA-seq data.

ESCA and CESC were stratified into squamous cell (SQ) and adeno- (AD) carcinomas.

For all boxplots, the top, middle and bottom line of the boxplot represent the upper quartile (Q3), median, and lower quartile (Q1) respectively. The maximum value represented by the top whisker represents the highest observed data point within Q3 + (1.5 x (Q3-Q1)), and the minimum value represented by the bottom whisker represents the lowest situated point within Q1 - (1.5 x (Q3-Q1)).

Figure EV3. *APOBEC3A* is positively correlated with differentiation marker genes and negatively correlated with proliferation marker genes in HNSCC cell lines.

A) Spearman's **c**orrelation of *APOBEC3A* expression with the expression of differentiation marker genes, proliferation marker genes, and genes of the RIPK4 pathway in 34 HNSCC cell

lines from the CCLE. P values calculated by T-test: *** = P < 0.0001; ** = P < 0.001; * = P < 0.05; . = P < 0.1.

B) Log2 expression levels of *APOBEC3A* and *GRHL3* in the 34 individual HNSCC cell lines from the CCLE. Accompanies Figure 5.

Figure EV4. Detection of APOBEC3A and APOBEC3B protein expression in HNSCC.

Representative images from an HNSCC tissue microarray stained with APOBEC3A-specific (left panels) or APOBEC3A/B/G-specific (right panels) antibodies. Accompanies Figure 5.

No. Cells
4355
11276
80489
2623
2649
23425
24489
12068
20323
19314
46497
44547
A3A Only
A3B Only
Both A3A & A3B
Neither A3A or A3B
Mean
Read Counts (log10 + 1)
APOBEC3A
APOBEC3B
0
1
2
3
Breast (N) Wu 2021
Lung (N) Madissoon 2020
Oesophagus (N) Madissoon 2020
Skin (N) Solé−Boldo 2020
Tonsil (N)
Bladder (T) Luo 2022
Breast (T) Wu 2021
Head and Neck (T) Kürten 2021
Head and Neck (T) Puram 2023
Head and Neck (T)
Lung (T) Prazanowska 2023
Oesophagus (T) Zhang 2021
Normal
Tumour

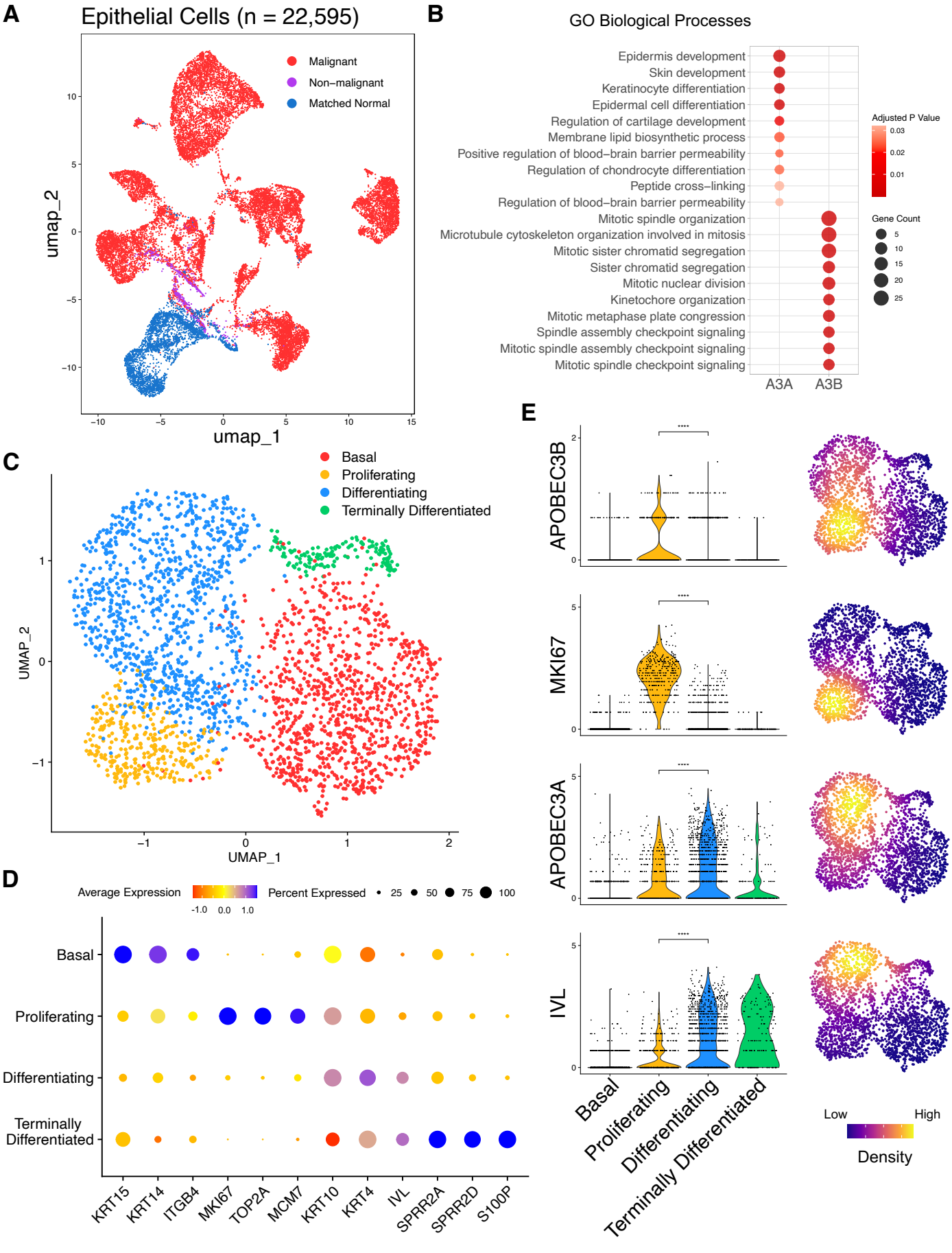
A
Epithelial Cells (n = 22,595)
Malignant
Non−malignant
Matched Normal
umap_2
umap_1
B
GO Biological Processes
Epidermis development
Skin development
Keratinocyte differentiation
Epidermal cell differentiation
Regulation of cartilage development
Membrane lipid biosynthetic process
Positive regulation of blood−brain barrier permeability
Regulation of chondrocyte differentiation
Peptide cross−linking
Regulation of blood−brain barrier permeability
Mitotic spindle organization
Microtubule cytoskeleton organization involved in mitosis
Mitotic sister chromatid segregation
Sister chromatid segregation
Mitotic nuclear division
Kinetochore organization
Mitotic metaphase plate congression
Spindle assembly checkpoint signaling
Mitotic spindle assembly checkpoint signaling
Mitotic spindle checkpoint signaling
A3A
A3B
Adjusted P Value
Gene Count
C
Basal
Proliferating
Differentiating
Terminally Differentiated
UMAP_2
UMAP_1
D
Average Expression
Percent Expressed
Basal
Proliferating
Differentiating
Terminally Differentiated
KRT15
KRT14
ITGB4
MKI67
TOP2A
MCM7
KRT10
KRT4
IVL
SPRR2A
SPRR2D
S100P
E
APOBEC3B
MKI67
APOBEC3A
IVL
Basal
Proliferating
Differentiating
Terminally Differentiated
Low
High
Density

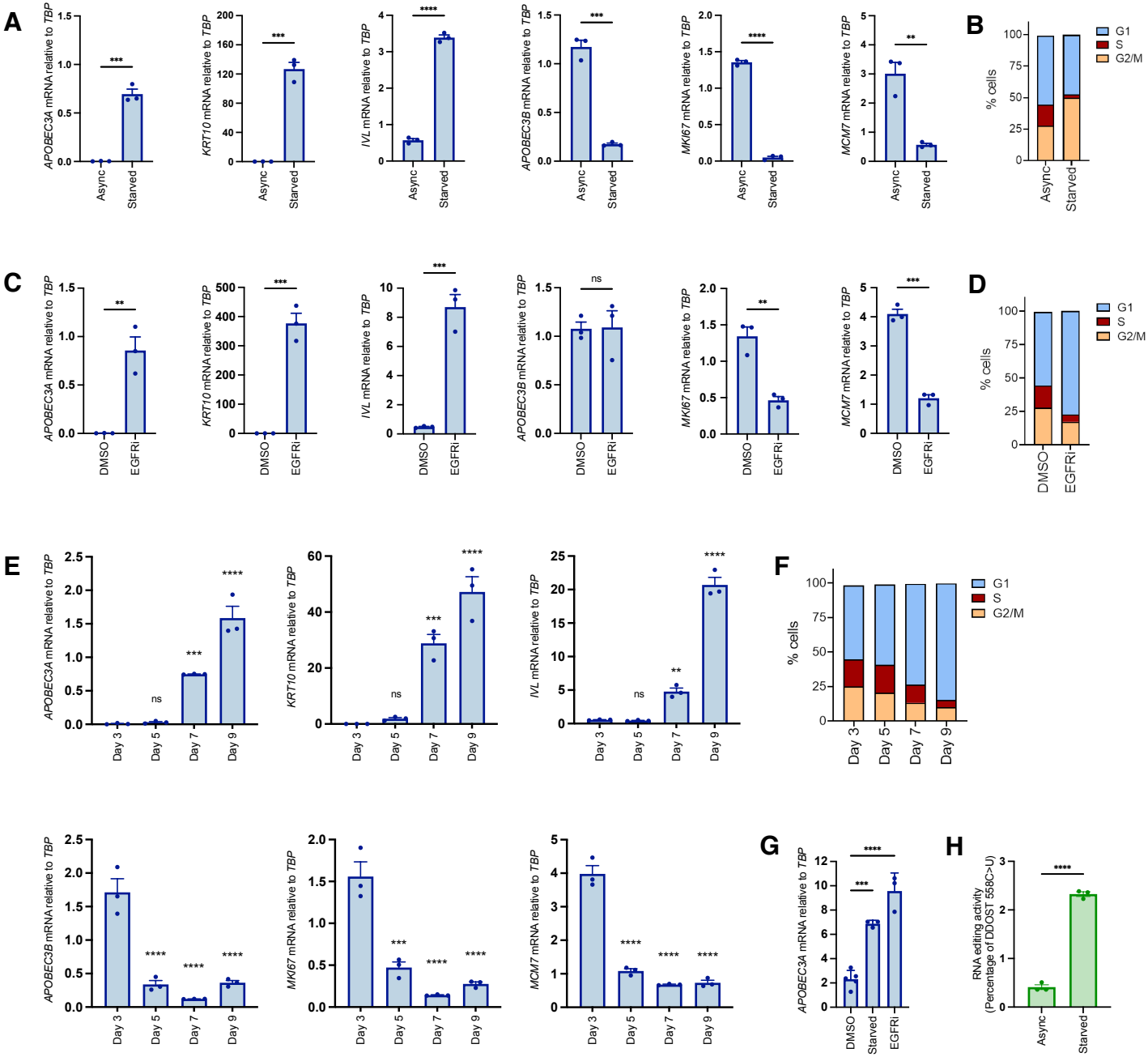
A
APOBEC3A mRNA relative to TBP
KRT10 mRNA relative to TBP
IVL mRNA relative to TBP
APOBEC3B mRNA relative to TBP
MKI67 mRNA relative to TBP
MCM7 mRNA relative to TBP
Async
Starved
B
% cells
G1
S
G2/M
C
DMSO
EGFRi
ns
D
E
Day 3
Day 5
Day 7
Day 9
F
G
H
RNA editing activity (Percentage of DDOST 558C>U)

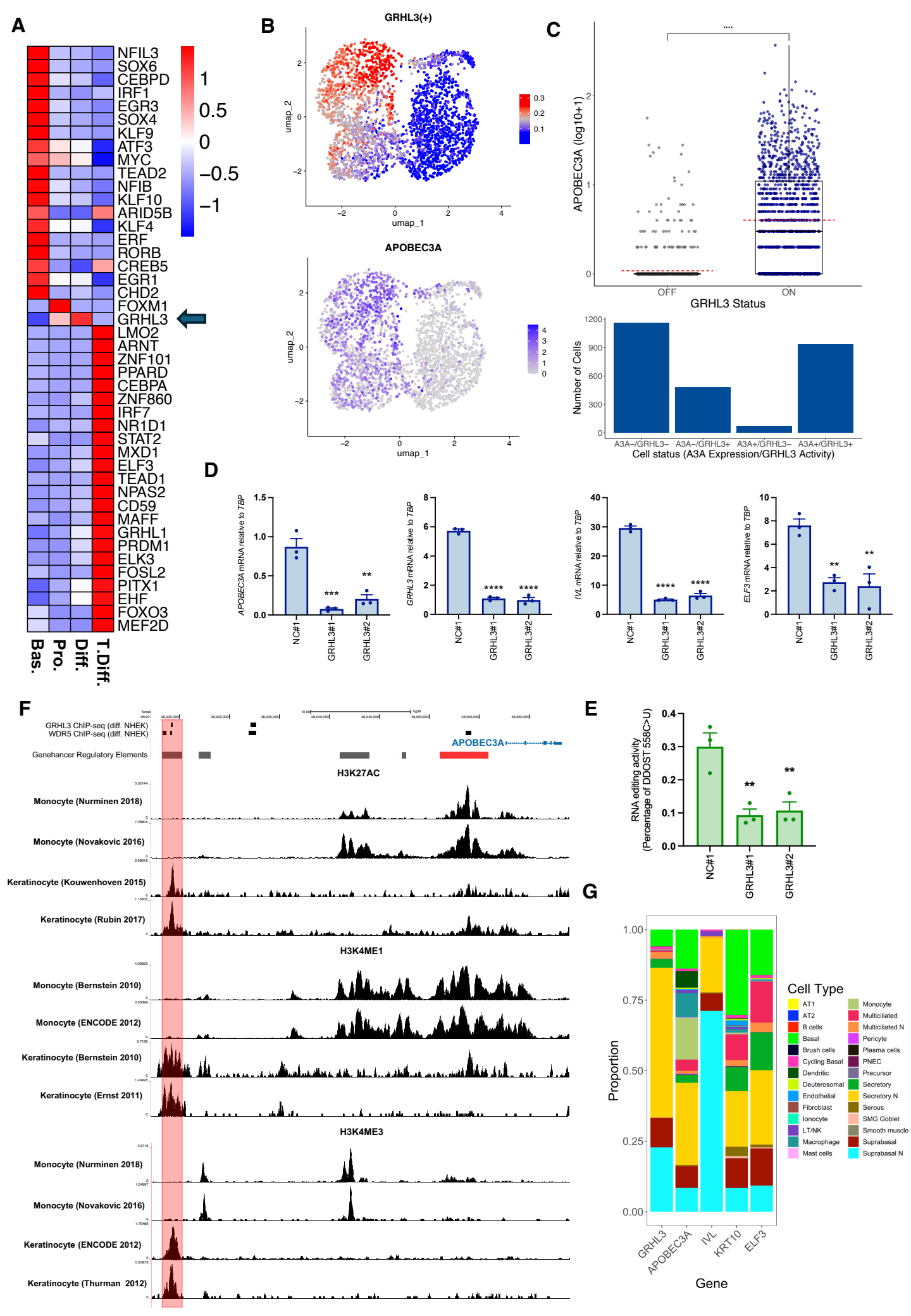
A
NFIL3
SOX6
CEBPD
IRF1
EGR3
SOX4
KLF9
ATF3
MYC
TEAD2
NFIB
KLF10
ARID5B
KLF4
ERF
RORB
CREB5
EGR1
CHD2
FOXM1
GRHL3
LMO2
ARNT
ZNF101
PPARD
CEBPA
ZNF860
IRF7
NR1D1
STAT2
MXD1
ELF3
TEAD1
NPAS2
CD59
MAFF
GRHL1
PRDM1
ELK3
FOSL2
PITX1
EHF
FOXO3
MEF2D
1
0.5
0
−0.5
−1
Bas.
Pro.
Diff.
T.Diff.
B
GRHL3(+)
umap_1
umap_2
APOBEC3A
C
APOBEC3A (log10+1)
OFF
ON
GRHL3 Status
Number of Cells
A3A−/GRHL3−
A3A−/GRHL3+
A3A+/GRHL3−
A3A+/GRHL3+
Cell status (A3A Expression/GRHL3 Activity)
D
APOBEC3A mRNA relative to TBP
GRHL3 mRNA relative to TBP
IVL mRNA relative to TBP
ELF3 mRNA relative to TBP
NC#1
GRHL3#1
GRHL3#2
E
RNA editing activity
(Percentage of DDOST 558C>U)
F
GRHL3 ChIP-seq (diff. NHEK)
WDR5 ChIP-seq (diff. NHEK)
Genehancer Regulatory Elements
APOBEC3A
H3K27AC
Monocyte (Nurminen 2018)
Monocyte (Novakovic 2016)
Keratinocyte (Kouwenhoven 2015)
Keratinocyte (Rubin 2017)
H3K4ME1
Monocyte (Bernstein 2010)
Monocyte (ENCODE 2012)
Keratinocyte (Bernstein 2010)
Keratinocyte (Ernst 2011)
H3K4ME3
Monocyte (Nurminen 2018)
Monocyte (Novakovic 2016)
Keratinocyte (ENCODE 2012)
Keratinocyte (Thurman 2012)
G
Proportion
Gene
GRHL3
APOBEC3A
IVL
KRT10
ELF3
Cell Type
AT1
AT2
B cells
Basal
Brush cells
Cycling Basal
Dendritic
Deuterosomal
Endothelial
Fibroblast
Ionocyte
LT/NK
Macrophage
Mast cells
Monocyte
Multiciliated
Multiciliated N
Pericyte
Plasma cells
PNEC
Precursor
Secretory
Secretory N
Serous
SMG Goblet
Smooth muscle
Suprabasal
Suprabasal N

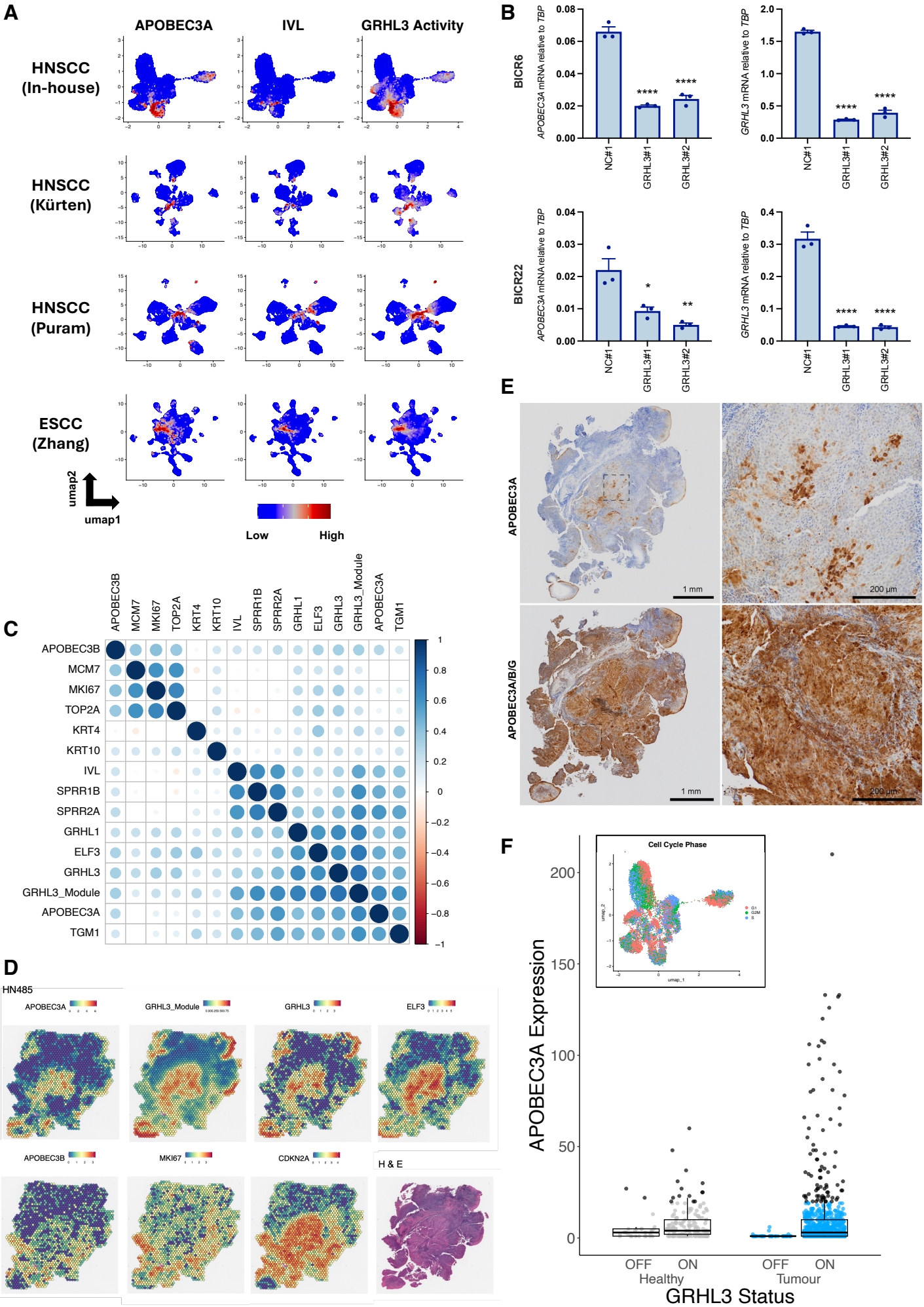
A
APOBEC3A
IVL
GRHL3 Activity
HNSCC (In-house)
HNSCC (Kürten)
HNSCC (Puram)
ESCC (Zhang)
umap2
umap1
Low
High
B
BICR6
BICR22
APOBEC3A mRNA relative to TBP
GRHL3 mRNA relative to TBP
NC#1
GRHL3#1
GRHL3#2
C
APOBEC3B
MCM7
MKI67
TOP2A
KRT4
KRT10
IVL
SPRR1B
SPRR2A
GRHL1
ELF3
GRHL3
GRHL3_Module
APOBEC3A
TGM1
D
HN485
APOBEC3A
GRHL3_Module
GRHL3
ELF3
APOBEC3B
MKI67
CDKN2A
H & E
E
APOBEC3A
APOBEC3A/B/G
1 mm
200 µm
F
Cell Cycle Phase
APOBEC3A Expression
OFF
ON
Healthy
Tumour
GRHL3 Status

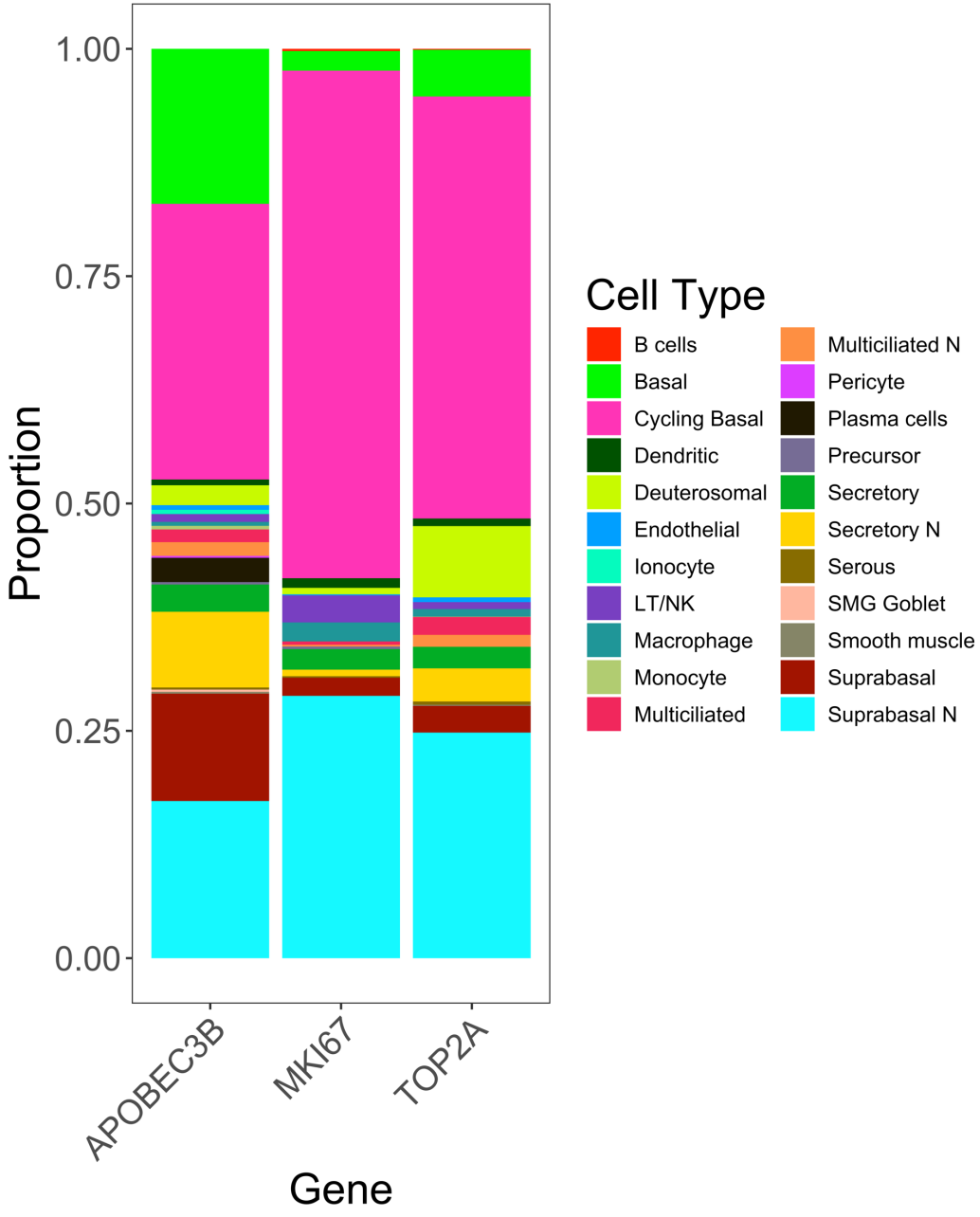
1.00
0.75
0.50
0.25
0.00
Proportion
APOBEC3B
MKI67
TOP2A
Gene
Cell Type
B cells
Basal
Cycling Basal
Dendritic
Deuterosomal
Endothelial
Ionocyte
LT/NK
Macrophage
Monocyte
Multiciliated
Multiciliated N
Pericyte
Plasma cells
Precursor
Secretory
Secretory N
Serous
SMG Goblet
Smooth muscle
Suprabasal
Suprabasal N

A

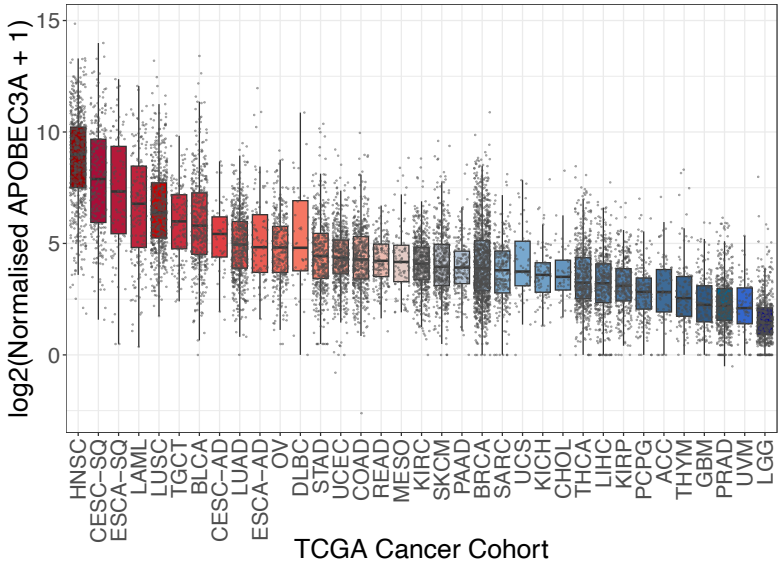

B

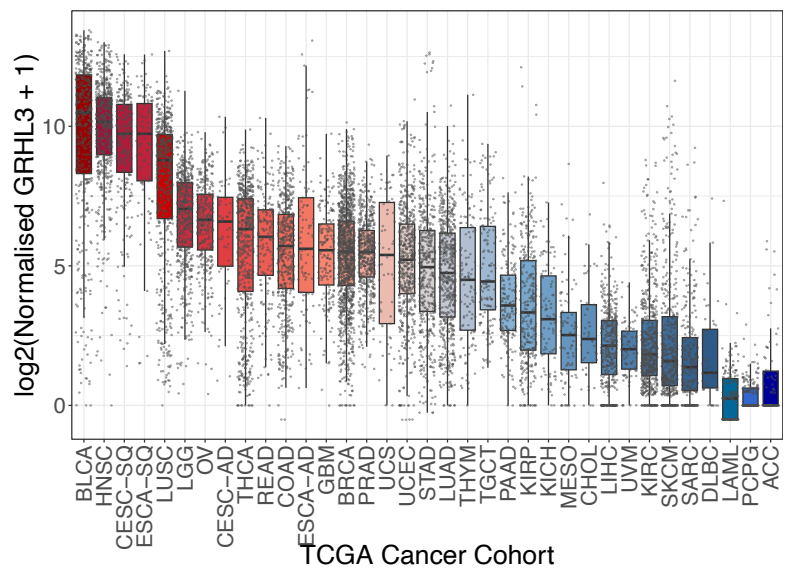

C

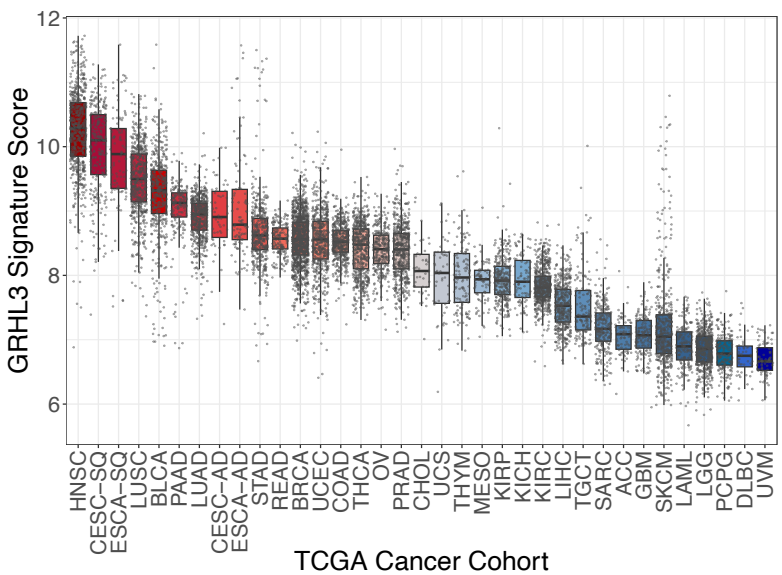

D

TCGA Cancer Type	n	Spearman Correlation	Adjusted p-value
ESCA-SQ	99	0.65	2.48E-12
CESC-SQ	255	0.62	2.10E-27
CESC-AD	54	0.51	2.70E-04
ESCA-AD	97	0.48	2.17E-06
THYM	122	0.47	2.15E-07
HNSC	566	0.43	2.31E-25
THCA	572	0.40	3.45E-22
LUSC	552	0.32	9.80E-14
PRAD	550	0.20	8.56E-06
BRCA	1,215	0.19	4.07E-10
CHOL	45	0.15	3.94E-01
OV	308	0.14	3.29E-02
BLCA	427	0.12	3.75E-02
KICH	91	0.10	4.36E-01
UCEC	555	0.09	7.62E-02
PAAD	183	0.07	3.94E-01
SKCM	473	0.06	2.59E-01
STAD	450	0.06	3.03E-01
LUAD	576	0.06	2.59E-01
LAML	173	0.00	9.64E-01
KIRP	323	0.00	9.64E-01
DLBC	48	-0.01	9.64E-01
LIHC	423	-0.01	8.49E-01
ACC	79	-0.03	8.49E-01
LGG	529	-0.12	2.05E-02
SARC	265	-0.12	1.06E-01
GBM	166	-0.12	1.96E-01
TGCT	139	-0.13	1.96E-01
PCPG	187	-0.13	1.30E-01
READ	170	-0.15	8.67E-02
COAD	492	-0.16	9.22E-04
KIRC	606	-0.16	1.75E-04
MESO	87	-0.23	6.60E-02

E

TCGA Cancer Type	n	Spearman Correlation	Adjusted p-value
ESCA-SQ	99	0.71	1.2E-15
CESC-SQ	255	0.68	3.7E-35
ESCA-AD	97	0.64	5.9E-12
CESC-AD	54	0.57	9.1E-06
LAML	173	0.56	3.3E-15
LUSC	552	0.54	3.9E-42
THYM	122	0.54	2.9E-10
HNSC	566	0.54	4.0E-42
THCA	572	0.53	5.9E-41
KICH	91	0.46	6.8E-06
BLCA	427	0.45	8.6E-22
DLBC	48	0.37	1.2E-02
SKCM	473	0.37	1.0E-15
SARC	265	0.34	2.2E-08
PRAD	550	0.32	4.7E-14
PCPG	187	0.31	2.9E-05
GBM	166	0.31	8.6E-05
LIHC	423	0.30	5.7E-10
LGG	529	0.28	2.3E-10
STAD	450	0.27	1.4E-08
OV	308	0.25	1.5E-05
LUAD	576	0.24	1.3E-08
COAD	492	0.24	1.7E-07
CHOL	45	0.22	1.7E-01
KIRP	323	0.22	1.1E-04
UCEC	555	0.18	1.8E-05
BRCA	1,215	0.17	2.0E-09
READ	170	0.16	4.6E-02
PAAD	183	0.07	3.3E-01
MESO	87	0.04	7.5E-01
TGCT	139	0.01	9.0E-01
KIRC	606	-0.07	8.6E-02
ACC	79	-0.16	1.8E-01

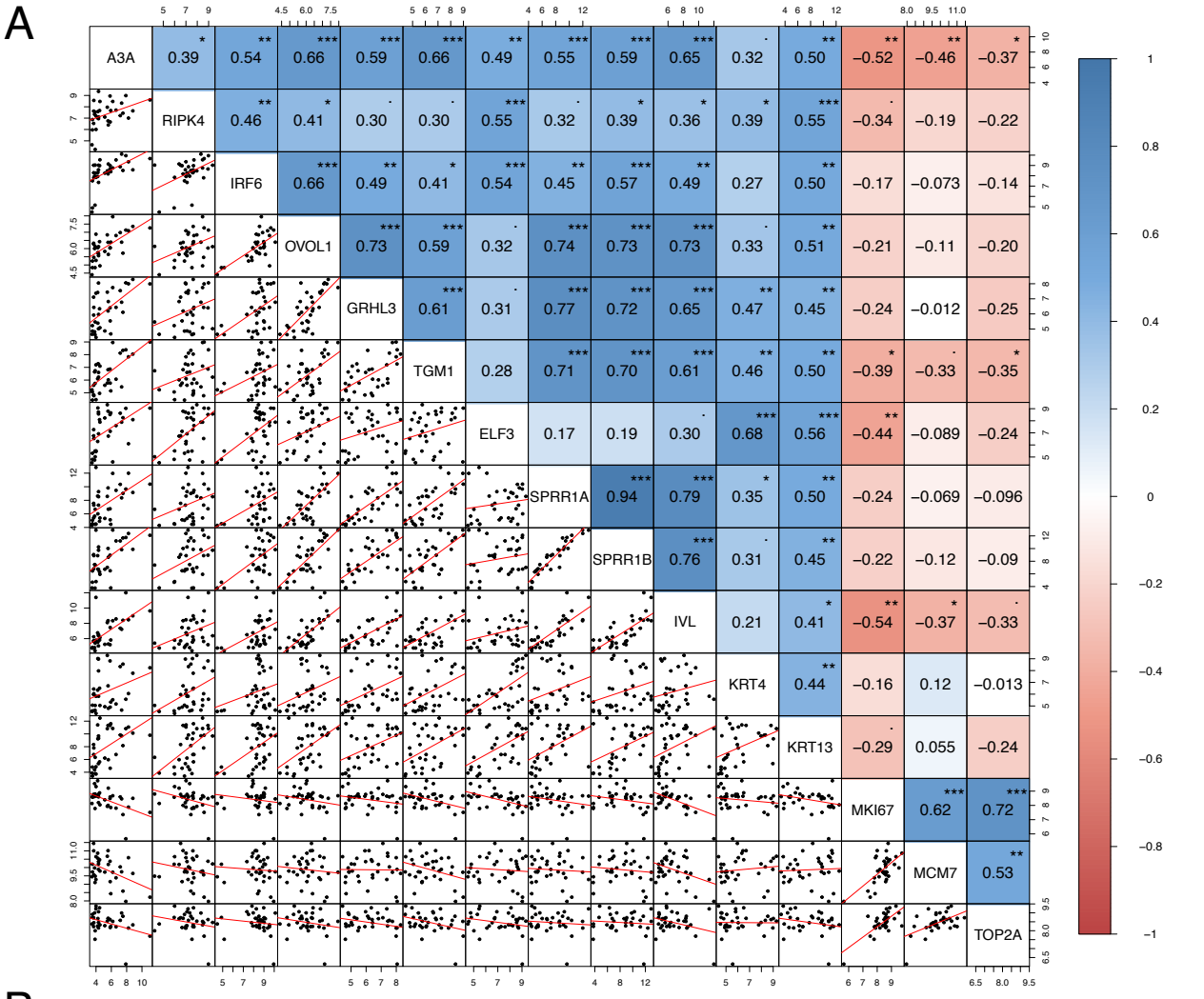
A
A3A
RIPK4
IRF6
OVOL1
GRHL3
TGM1
ELF3
SPRR1A
SPRR1B
IVL
KRT4
KRT13
MKI67
MCM7
TOP2A
1
0.8
0.6
0.4
0.2
0
−0.2
−0.4
−0.6
−0.8
−1

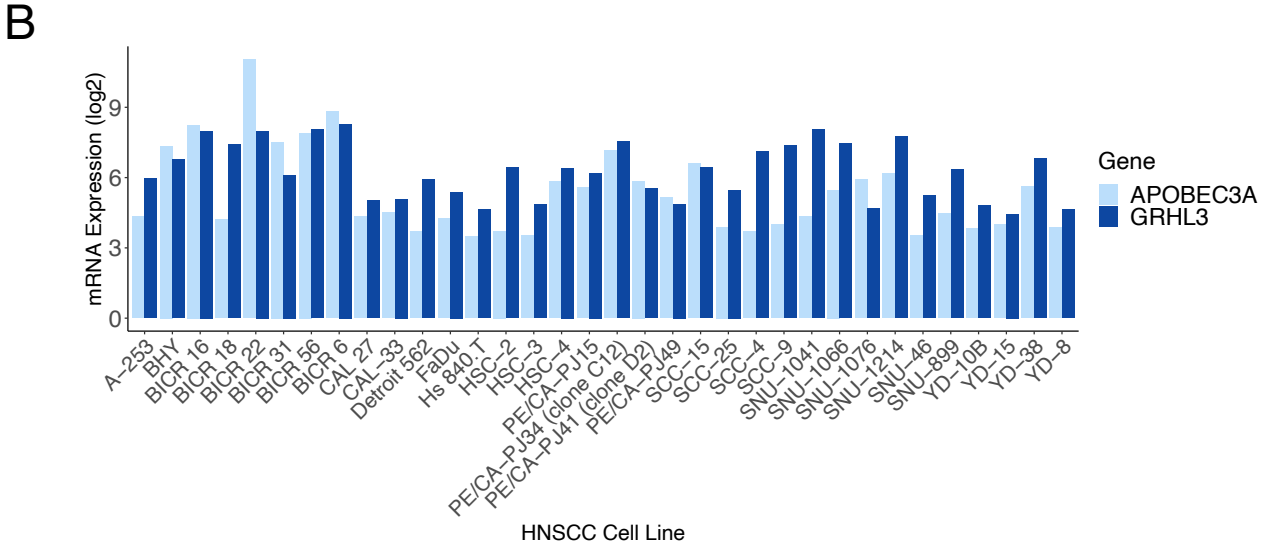
B
mRNA Expression (log2)
0
3
6
9
A−253
BHY
BICR 16
BICR 18
BICR 22
BICR 31
BICR 56
BICR 6
CAL 27
CAL−33
Detroit 562
FaDu
Hs 840.T
HSC−2
HSC−3
HSC−4
PE/CA−PJ15
PE/CA−PJ34 (clone C12)
PE/CA−PJ41 (clone D2)
PE/CA−PJ49
SCC−15
SCC−25
SCC−4
SCC−9
SNU−1041
SNU−1066
SNU−1076
SNU−1214
SNU−46
SNU−899
YD−10B
YD−15
YD−38
YD−8
HNSCC Cell Line
Gene
APOBEC3A
GRHL3

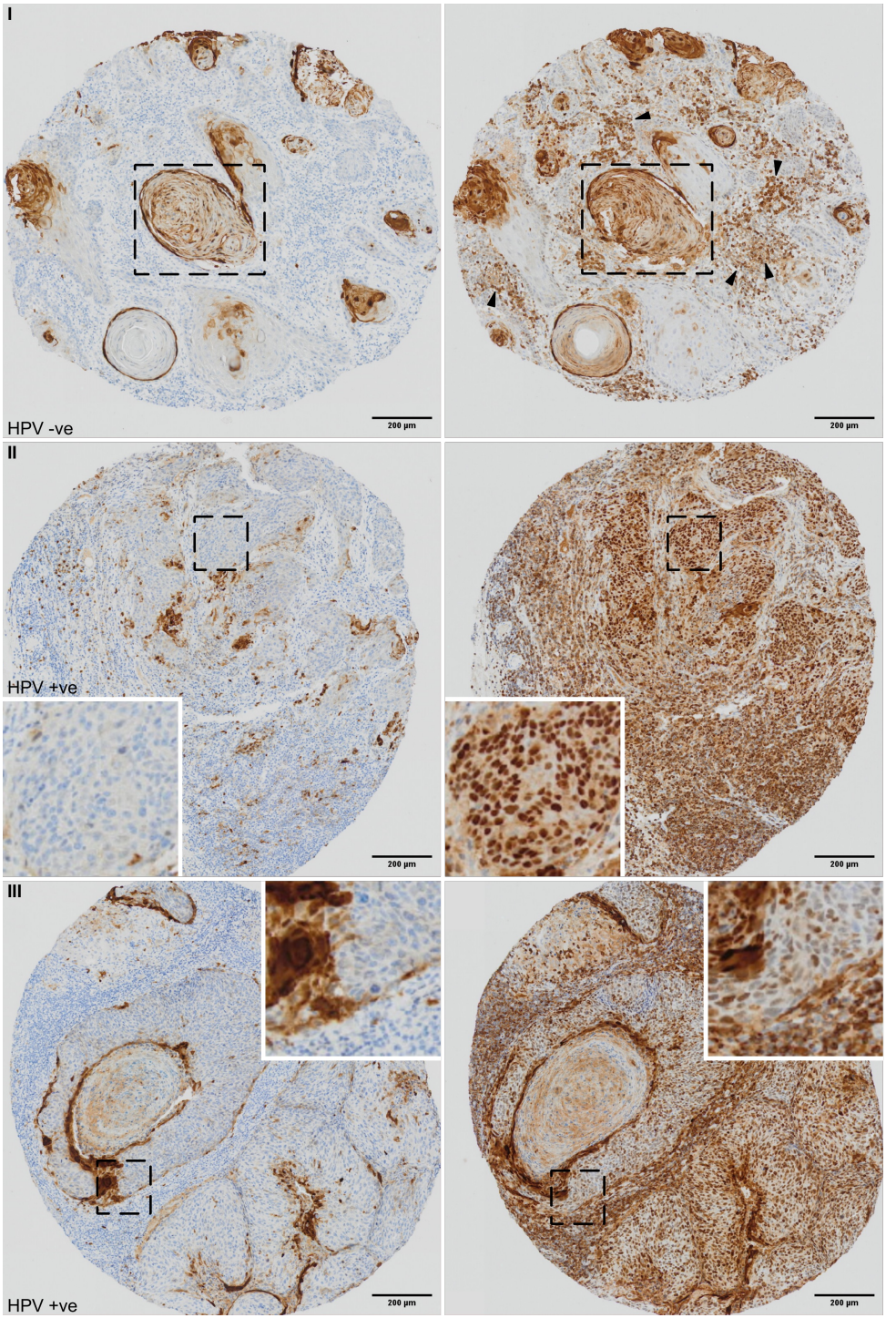
APOBEC3A
APOBEC3A/B/G
I
HPV -ve
200 µm
200 µm
II
HPV +ve
200 µm
200 µm
III
HPV +ve
200 µm
200 µm